RADC-TR-78-87
Final Technical Report
April 1978

TWO FORTRAN PROGRAMS FOR CALCULATING GLOBAL IONOSPHERIC AMPLITUDE AND PHASE SCINTILLATION

Stanford Research Institute

Sponsored by
Defense Advanced Research Projects Agency (DoD)
ARPA Order No. 2777

ROME AIR DEVELOPMENT CENTER
Air Force Systems Command
Griffiss Air Force Base, New York 13441

This report has been reviewed by the RADC Information Office (OI) and is releasable to the National Technical Information Service (NTIS). At NTIS it will be releasable to the general public, including foreign nations.

RADC-TR-78-87 has been reviewed and is approved for publication.

APPROVED: Richard A Schneible

RICHARD A. SCHNEIBLE
Project Engineer

If your address has changed or if you wish to be removed from the RADC mailing list, or if the addressee is no longer employed by your organization, please notify RADC (OCSA), Griffiss AFB NY 13441. This will assist us in maintaining a current mailing list.

Do not return this copy. Retain or destroy.

TWO FORTRAN PROGRAMS FOR CALCULATING GLOBAL IONOSPHERIC AMPLITUDE AND PHASE SCINTILLATION

Charles L. Rino
Edward J. Fremouw
Anne R. Hessing
V. Elaine Hatfield

Contractor: Stanford Research Institute
Contract Number: F30602-75-C-0236
Effective Date of Contract: 15 May 1975
Contract Expiration Date: 14 July 1977
Short Title of Work: Continued Modeling of Trans-ionospheric Propagation
Program Code Number: 7E20
Period of Work Covered: May 76 - Jul 77

Principal Investigator: Dr. Edward J. Fremouw
Phone: (415) 326-6200, Ext. 2596

Project Engineer: Mr. Richard A. Schneible
Phone: (315) 330-2814

This research was supported by the Defense Advanced Research Projects Agency of the Department of Defense and was monitored by Mr. Richard A. Schneible (OCSA), Griffiss AFB NY 13441 under Contract F30602-75-C-0236.

UNCLASSIFIED

SECURITY CLASSIFICATION OF THIS PAGE (When Data Entered)

REPORT DOCUMENTATION PAGE	READ INSTRUCTIONS BEFORE COMPLETING FORM
1. REPORT NUMBER: RADC-TR-78-87	2. GOVT ACCESSION NO. / 3. RECIPIENT'S CATALOG NUMBER
4. TITLE (and Subtitle): TWO FORTRAN PROGRAMS FOR CALCULATING GLOBAL IONOSPHERIC AMPLITUDE AND PHASE SCINTILLATION	5. TYPE OF REPORT & PERIOD COVERED: Final Technical Report, 15 May 76 - 15 July 77
	6. PERFORMING ORG. REPORT NUMBER: SRI Project 4259
7. AUTHOR(s): Charles L. Rino, Anne R. Hessing, Edward J. Fremouw, V. Elaine Hatfield	8. CONTRACT OR GRANT NUMBER(s): F30602-75-C-0236, ARPA Order 2777
9. PERFORMING ORGANIZATION NAME AND ADDRESS: Stanford Research Institute, Menlo Park CA 94025	10. PROGRAM ELEMENT, PROJECT, TASK AREA & WORK UNIT NUMBERS: 62301E, 27770102
11. CONTROLLING OFFICE NAME AND ADDRESS: Defense Advanced Research Projects Agency, 1400 Wilson Blvd, Arlington VA 22209	12. REPORT DATE: Apr 78
	13. NUMBER OF PAGES: 68 (12 67p.)
14. MONITORING AGENCY NAME & ADDRESS (if different from Controlling Office): Rome Air Development Center (OCSA), Griffiss AFB NY 13441	15. SECURITY CLASS. (of this report): UNCLASSIFIED
	15a. DECLASSIFICATION/DOWNGRADING SCHEDULE: N/A
16. DISTRIBUTION STATEMENT (of this Report): None	(16) 2777 (17) 01
17. DISTRIBUTION STATEMENT (of the abstract entered in Block 20, if different from Report): None	
18. SUPPLEMENTARY NOTES: RADC Project Engineer: Mr. Richard Schneible (OCSA)	
19. KEY WORDS (Continue on reverse side if necessary and identify by block number): Ionospheric scintillation, Fading, Computer models	

20. ABSTRACT (Continue on reverse side if necessary and identify by block number)

This report contains detailed descriptions of the FORTRAN computer codes *IONSCNT*, which calculates average ionospheric amplitude and phase scintillation conditions on a global basis, and the auxiliary statistics program DIST, which uses the IONSCNT outputs to calculate fading statistics. Operating instructions for the programs together with examples and descriptions of the various outputs are included. The theoretical background and data base for the program development is contained in a separately published report (Fremouw et al., 1977).

DD FORM 1 JAN 73 1473 EDITION OF 1 NOV 65 IS OBSOLETE

UNCLASSIFIED

SECURITY CLASSIFICATION OF THIS PAGE (When Data Entered)

332500

CL

CONTENTS

ILLUSTRATIONS

TABLES

I INTRODUCTION

In this report the organization and operation of the FORTRAN computer code IONSCNT, which calculates average ionospheric amplitude and phase scintillation conditions on a global basis, is described together with the auxiliary statistics program DIST. IONSCNT is a completely revised version of an earlier computer code (Fremouw and Rino, 1975, 1976).* A detailed discussion of the theory and experimental data base that was used in developing the new code is presented in Quarterly Technical Report 7 on this contract (Fremouw et al., 1977).

As with the earlier version of the code, IONSCNT is built around an empirically derived global rms electron density model. The user specifies the signal source and receiver locations together with the day number, time, sunspot number, and planetary magnetic index K_p. Any input parameter can be varied with a predetermined increment and range. In addition, to simulate an orbiting satellite the user of IONSCNT can vary the source location along a nominal circular orbit between two specified points on the earth. This provides a reasonable approximation to any satellite orbit over a short distance.

The principal output of IONSCNT consists of a tabular list of phase and amplitude scintillation indices together with a set of parameters that can be used in DIST to compute the complete first-order signal statistics. In addition, IONSCNT will generate intensity and phase autocorrelation functions for a selected subset of the data points computed during any run. Finally, IONSCNT will calculate the intensity correlation function for signals at two separated frequencies.

In the remainder of this report we shall present a detailed description of IONSCNT and instructions for its operation together with examples

---

* References are listed at the end of this report.

to illustrate the various program options. A user interested only in the program operation may wish to skip to Section III. For convenience, the mathematical computations that are performed in each subroutine are described in the Appendix. The auxiliary program DIST is described in Section IV.

II DESCRIPTION OF IONSCNT

A. General

A general flow diagram for IONSCNT is shown in Figure 1. From the specified locations of the signal source and receiver, the location of the ionospheric penetration point at the height of the irregularity layer is computed together with the propagation angles relative to the local geomagnetic coordinate system shown in Figure 2.

The rms electron density model effectively gives the intensity of the ionospheric turbulence for the particular location, season, time, and magnetic activity level. The rms electron density model also determines the values of the anisotropy parameters, a, b, δ, and the outer scale size for the focus component, α_f. The outer scale for the scatter component, α_s, is scaled from α_f (see Appendix, Section 1). The separation scale β_f is a fixed fraction of α_f such that $\beta_f > \alpha_s$.

Separate diffraction calculations are performed for the focus component in which a near-zone approximation is made and for the scatter component in which a full diffraction calculation is performed. The full diffraction calculation is very inefficient for large scale sizes. Thus, a near-zone approximation is used for the focus component to speed up the calculation.

The outputs of the separate scatter and focus diffraction calculations are combined to generate the first-order moments (I, in Figure 1) for all data points. For a selected subset of the data points, the second-order moments (II, in Figure 2) for phase and intensity can be computed. Two-frequency correlation functions for intensity are computed with special calls to the first-order time statistics subroutines.

To calculate the second-order autocorrelation functions, it is necessary to specify the drift rate of the ionosphere as well as any relative source motion. An ionospheric drift rate value is provided by

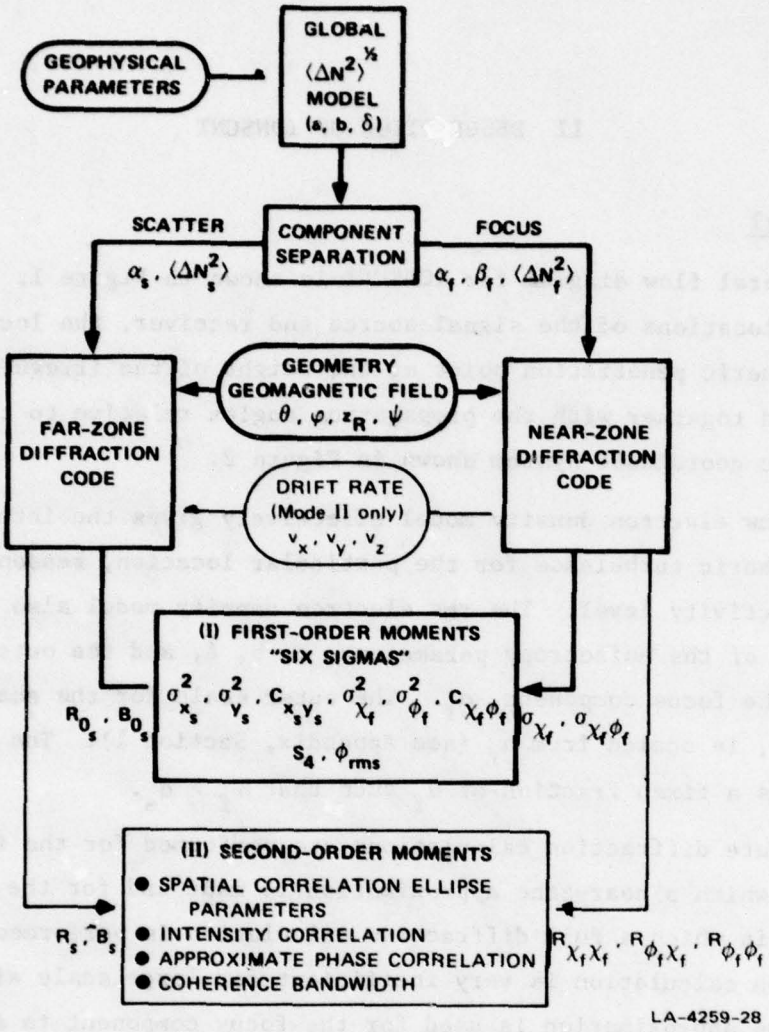

FIGURE 1 FLOW DIAGRAM OF IONSCNT

the global rms electron density model. The user can modify the model value if he so desires. Representative satellite velocities are computed whenever the nominal orbit code is utilized.

The most time-consuming operation is the scatter-component diffraction calculation. A full two-dimensional numerical integration is performed for each data point. The actual integration is done in polar coordinates with the integration over the angular coordinate performed

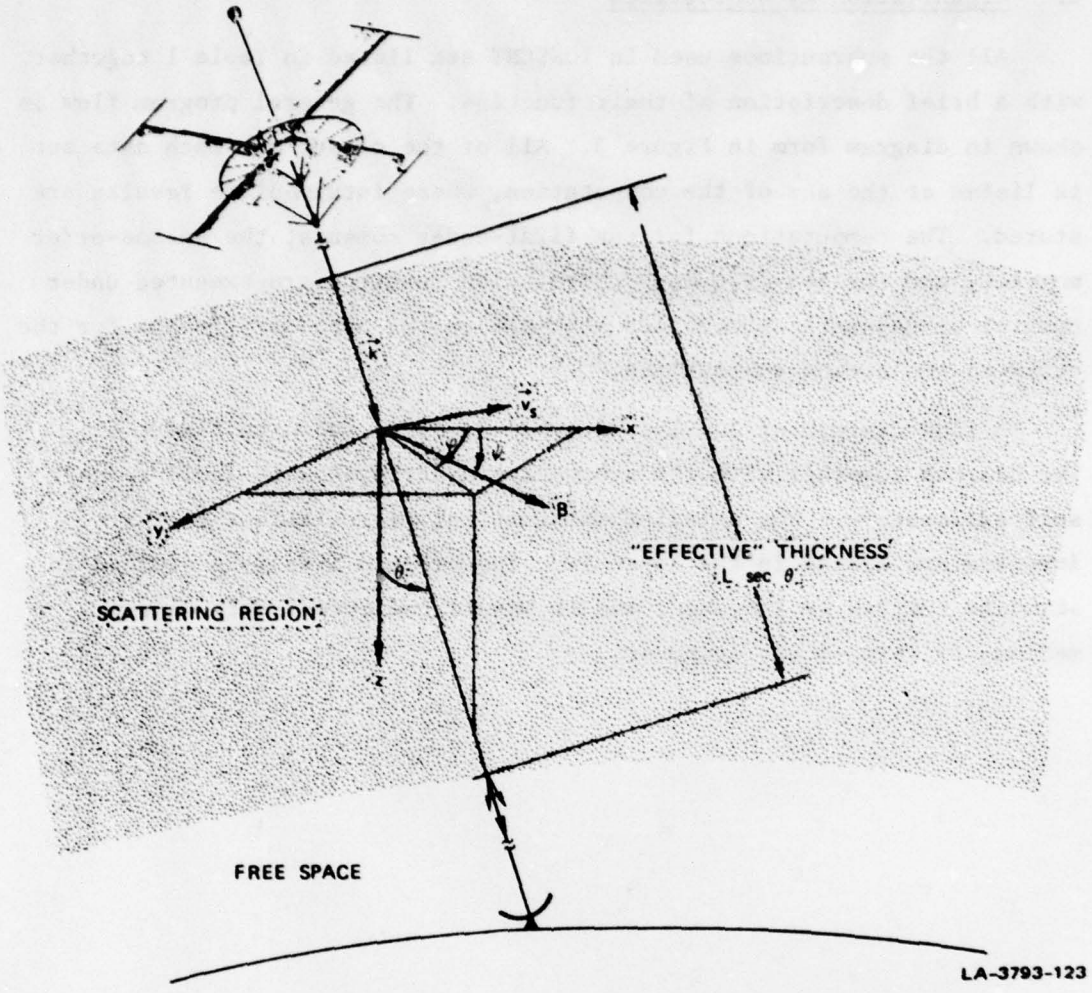

FIGURE 2 GEOMETRY FOR DIFFRACTION CALCULATIONS

only once for a fixed set of values over the radial coordinate. Thereafter, spline interpolation is used to generate the integrand for the integration over the radial variable (see Appendix A, Section 2).

The same integration is performed for both the first- and second-order statistics. For the latter, however, the separation variable is nonzero, and the integration converges much more slowly. Autocorrelation function values that have not converged after a specified number of terms are marked with an asterisk on the output list.

B. Organization by Subroutines

All the subroutines used in IONSCNT are listed in Table 1 together with a brief description of their function. The general program flow is shown in diagram form in Figure 3. All of the output for each data set is listed at the end of the computation, where intermediate results are stored. The computations for the first-order moments, the second-order moments, and the two-frequency correlation function are executed under control of separate subroutines that set up the necessary inputs for the calls to the common subroutines.

A flow diagram of IONSCNT by subroutines is shown in Figure 4. The diagram together with the subroutine descriptions in Table 1 are self explanatory. The detailed mathematical manipulations that are involved are listed in the Appendix. The program itself is written in standard FORTRAN IV language, and it should run efficiently on any medium- to large-scale computer.

Table 1

SUBROUTINES USED IN IONSCNT

Name	Definition
IONSCNT	Executive routine.
READIN, with ENTRY INC	Performs program input and increments the changing parameter(s)
FINDORB	Finds circular orbit at a given height through two points.
SRCHT	Finds orbital phase.
SRCHH	Finds hour angle of orbital plane.
SLAT	Calculates satellite latitude.
SLON	Calculates satellite longitude.
VXYZ	Calculates scan velocity.
ANGSD	Plane trigonometry routine.
MDLPRM	Sets and calculates model parameters.
SCINT1	Sets up inputs and calls to calculate first-order signal moments.
COORD	Finds point 2 given point 1 and azimuth and great-circle angle.
AZNGCA	Finds azimuth and great-circle angle from point 1 to point 2.
MGFLD	Calculates the geomagnetic coordinates of, and the field components at, a specified point using an earth-centered, axially tipped dipole model of the geomagnetic field.
RMSDN	Contains the worldwide model for strength of F-layer irregularities used in the scintillation calculation.
FINDZ	Computes the reduced distance from scattering layer to receiver for use in evaluating Fresnel-zone radius.
SIGCOM1	Provides calls for computation of the "six sigmas," S_4, and PRMS.
SIGF	Computes complex field moments for focus component.
RFOC	Computes higher-order derivatives of phase autocorrelation function for focus component.

Table 1 (Concluded)

Name	Definition
SIGS	Computes complex field moments for scatter component.
ABC	Computes anisotropy coefficients for phase ACF.
BRBIVL	Integrates asymmetry correlation function for scatter component.
COEFSP2	Computes spline coefficients for $G(\omega)$.
F	Computes integrand for polar integration over ray variable and angle variable.
G	Computes integrand for polar integration over ray variable from spline coefficients.
CPRMS	Controls calculation of rms phase.
PHAS, with ENTRY PRT	Evaluates the Hatfield phase distribution of a scintillating signal.
ERF	Computes the error function.
F1, with ENTRY F2	Provides integral functions for evaluating moments of phase distribution.
TWOFREQ	Sets up calling sequence for two-frequency correlation computation.
SCINT2	Sets up inputs and calculates second-order moments.
ELPSPRM	Calculates axial ratio and orientation angle for spatial autocorrelation function.
ELPRJCT	Transforms coordinates from plane normal to propagation vector to receiver plane.
SIGCOM2	Provides calls for computation of second-order moments.
SIMPA	Adaptively performs numerical integration using Simpson's rule.
SPLINE	Calculates coefficients for spline interpolation.
BESK	Computes the K Bessel Function for a given argument and order.
ASIN	Inverse sine routine.
ACOS	Inverse cosine routine.
ORDR1OP	Outputs first-order results.
ORDR2OP	Outputs second-order results.

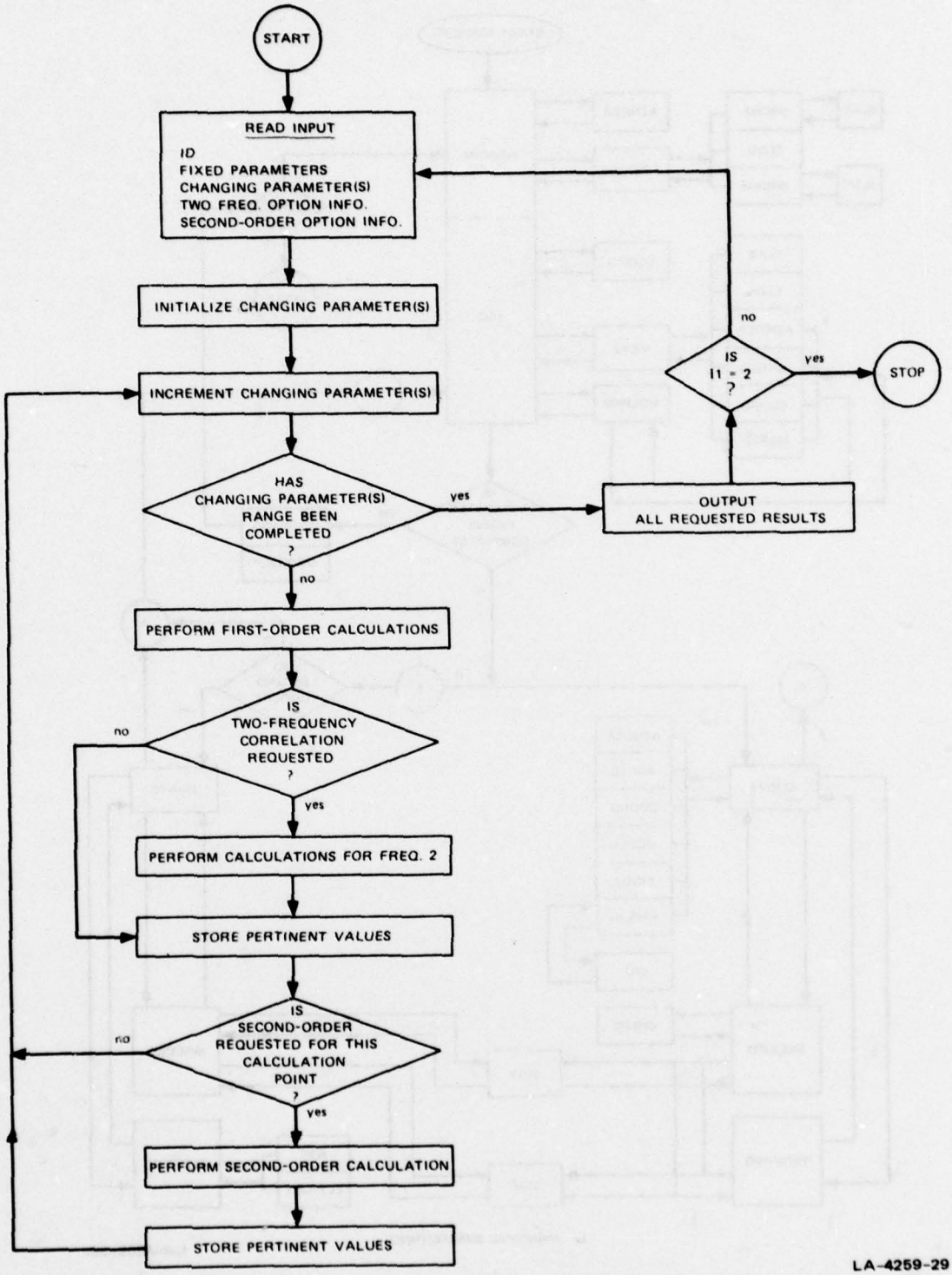

FIGURE 3 FLOW DIAGRAM FOR CONTROL OF IONSCNT

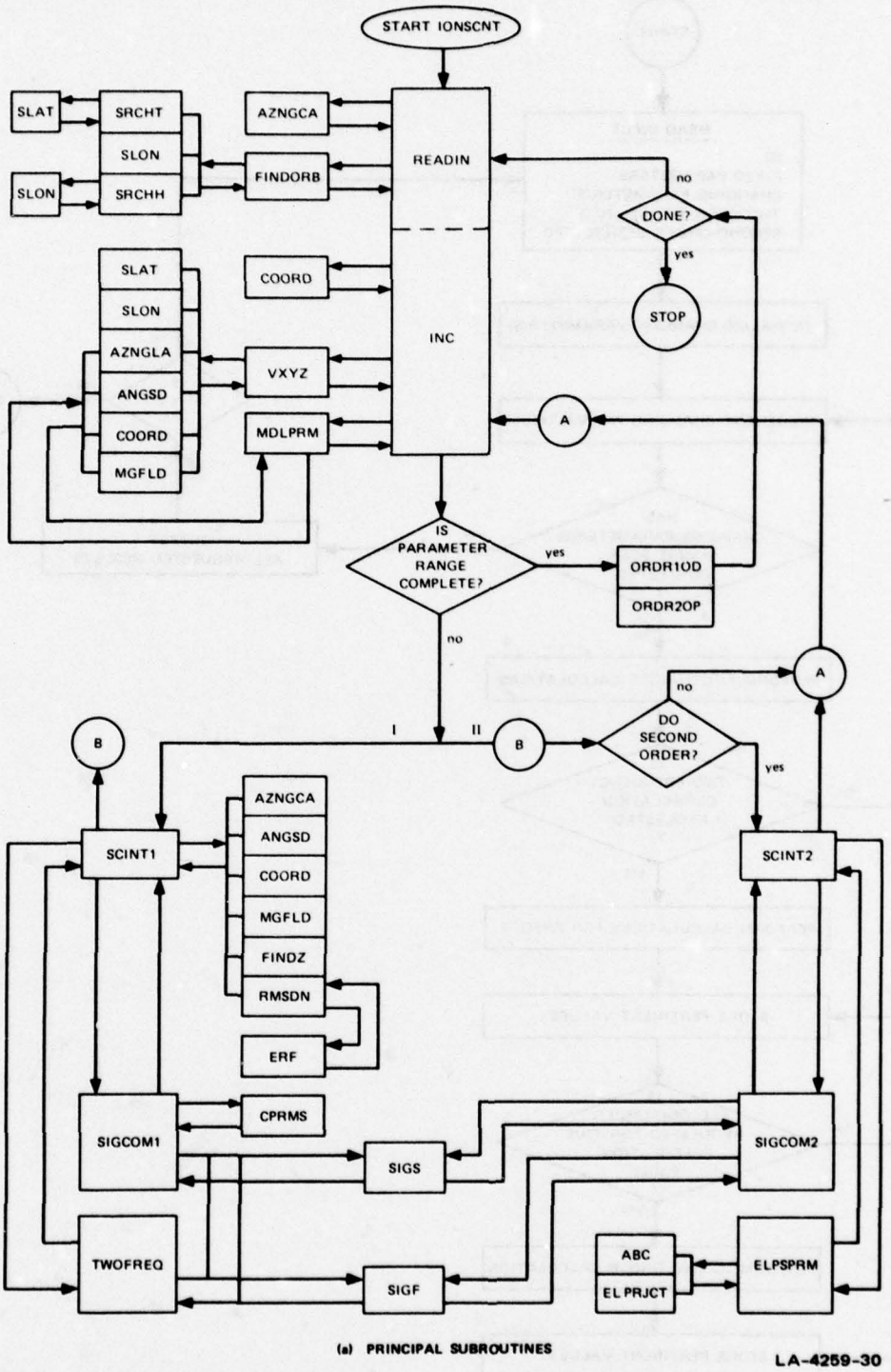

(a) PRINCIPAL SUBROUTINES

LA-4259-30

FIGURE 4 IONSCNT FLOW DIAGRAM BY SUBROUTINES

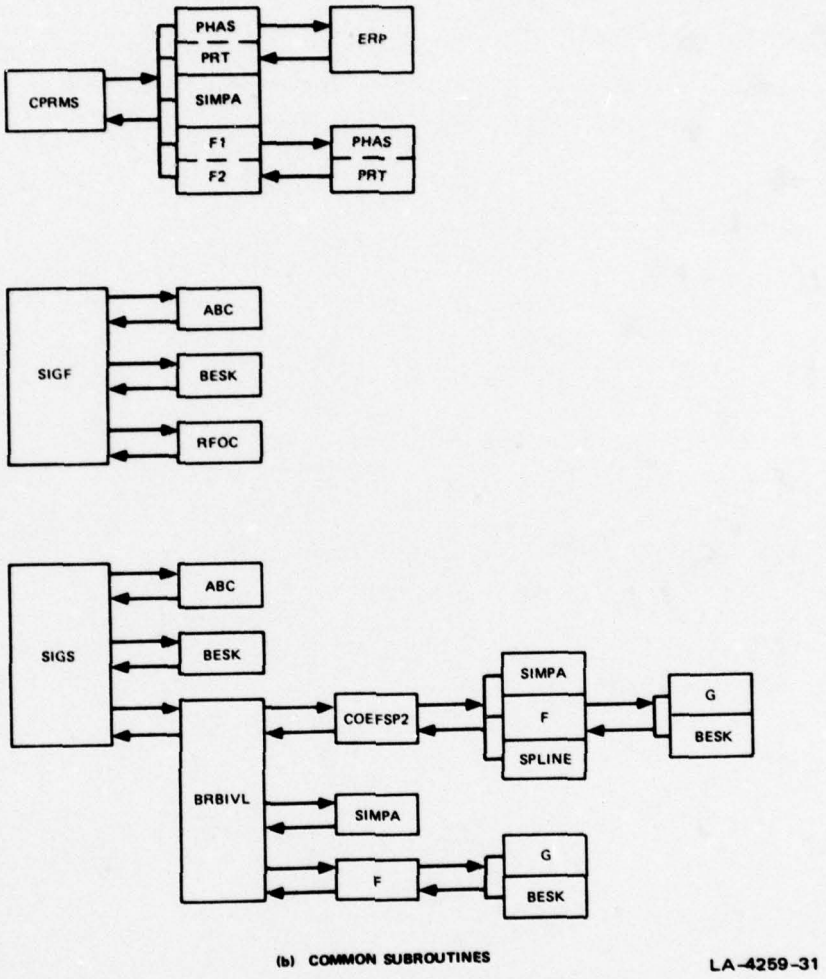

(b) COMMON SUBROUTINES

LA-4259-31

FIGURE 4 (Concluded)

III INSTRUCTIONS FOR USE OF IONSCNT

A. Program Inputs

To run IONSCNT it is necessary to prepare three types of input cards: (1) a title card, (2) namelist cards, and (3) a changing-parameter(s)/options card. Each type of card is described below. Three sample sets of input cards are shown in Figure 5.

The title card is used to assign any desired title of up to 80 characters to a specific case or series of cases. It is read by the executive program, IONSCNT, and printed on the output. It has no effect on the calculation. Any number of cases can be run under a common title.

The namelist cards are used to input the fixed parameters for a calculation case. They are read by subroutine READIN, by means of the namelist INPAR. The user gives the name and desired value for each quantity listed above the dashed line in Table 2 that is to remain fixed. The number under the heading K in the table is a program index used to identify the parameters. The user may list the fixed parameters in any order on the namelist cards. A parameter input on a namelist card will keep the specified value until changed by means of a new namelist card or until input on a changing parameter(s)/options card.

The first column of each namelist card must be blank. Columns 2 through 7 of the first entry in a sequence must be $INPAR. All namelist cards except the last must end with a constant followed by a comma. The last in a sequence must terminate with $.

The changing-parameter(s)/options card contains three types of information: (1) the independent variable(s) for a given calculation case, (2) the second frequency for the two-frequency correlation calculation, and (3) the information for second-order-statistics calculations. If neither (2) nor (3) is desired, this card returns to the form of the changing-parameter(s) card of previous versions of the program.

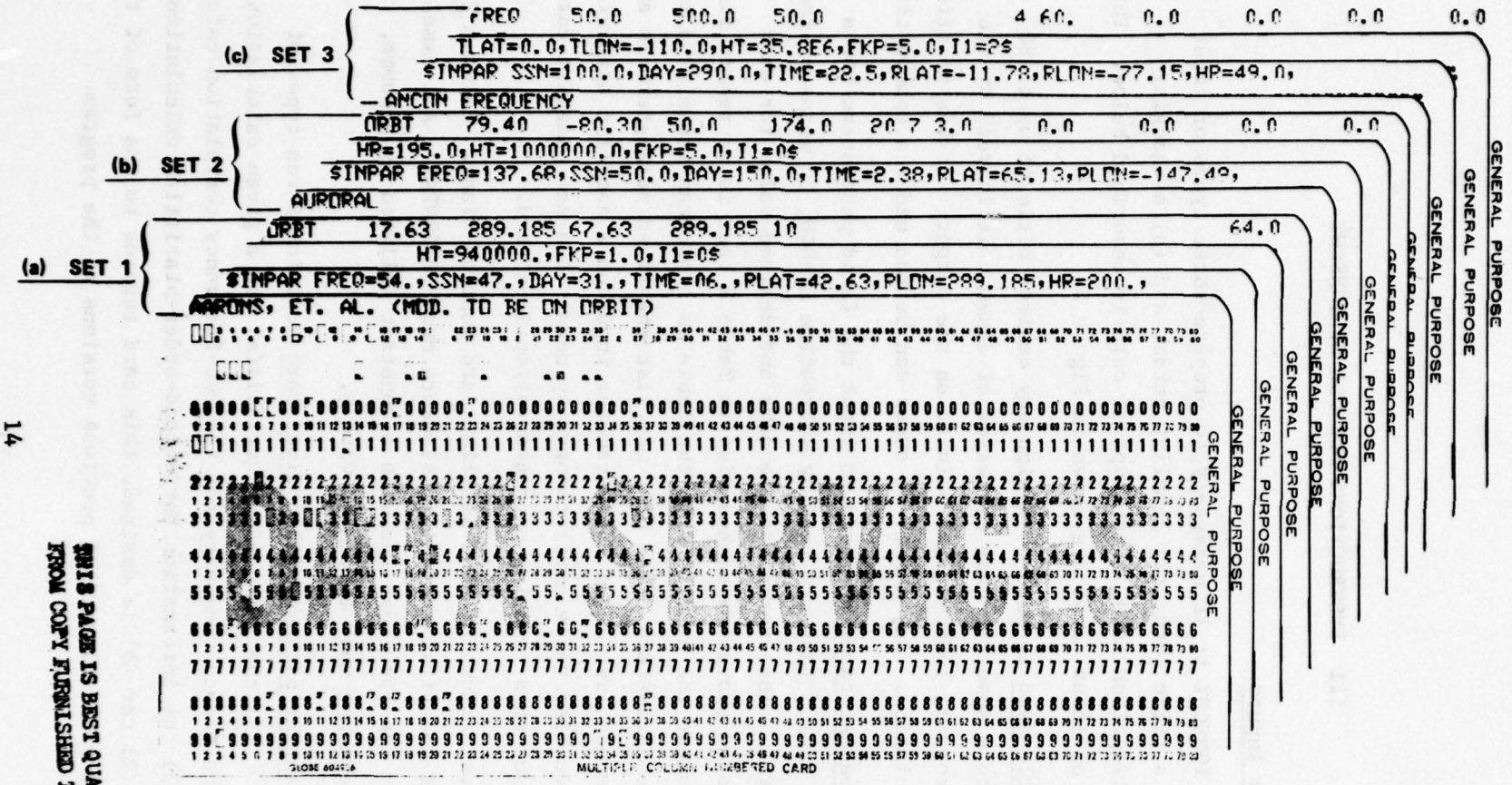

LA-4259-32

FIGURE 5 SAMPLE CARD INPUTS FOR IONSCNT

Table 2

DATA-CARD VARIABLES

K	Variable Name	Definition
1	FREQ	Frequency (MHz)
2	SSN	Sunspot number
3	DAY	Day of year
4	TIME*	Meridian time at the receiver (decimal hours)
5	RLAT	Receiver latitude (decimal degrees)
6	RLON	Receiver longitude (decimal degrees) (+east)
7	HR	Receiver altitude (meters)
8	TLAT	Transmitter latitude (decimal degrees)
9	TLON	Transmitter longitude (demical degrees) (+east)
10	HT	Transmitter altitude (meters)
11	FKP	Planetary magnetic index, K_p (0.0 through 9.0)
12	--	Not implemented
--	I1	Data flag = 0.1, or 2 (see text)
13	RCRD	Receiver coordinates (decimal degrees)
14	TCRD	Transmitter coordinates (decimal degrees)
15	ORBT	Transmitter coordinates (decimal degrees)

* Note that TIME has assumed a different definition from the definition that was used in previous versions of the program. It is now meridian time at the receiver. In the case where ORBT is the changing-parameter indicator, TIME is meridian time at the receiver for the first orbit point.

(See Table 2 regarding TIME exception.) The absence of additional entries indicates that the added calculations are to be suppressed.

If the variable named on the changing-parameter(s) card corresponds to a K value in Table 2 between 1 and 12, the calculation will be performed as a function of that single changing parameter. If RCRD (or TCRD) is specified, receiver (or transmitter) position will be incremented along a great-circle arc; thus the calculations will be dependent upon the variation of both a latitude and a longitude. If ORBT is specified, the transmitter will move (latitude and longitude) along a circular orbit at a fixed altitude (HT).

The parameters that have been added to the changing-parameter(s)/ options card relate to the two-frequency correlation calculation and to the second-order-statistics calculations. Their formats can be seen in Table 3. If FREQ2 = 0.0, the two-frequency correlation option is bypassed; otherwise, the value is the second frequency.

If NSCND $\leq$ 0, the second-order calculations are bypassed. NSCND = 1 gives second-order output for all calculation points; NSCND = 2 gives it for points 1, 3, 5, ...; NSCND = 3 gives it for points 1, 4, 7, ...; etc. Second-order calculations are done for 11 points from time lag = 0.0 to DLTMMX seconds. If DLTMMX $\leq$ 0.0, only the second-order heading information is given, but no detailed second-order moment calculations are performed. If the changing-parameter option is ORBT, the scan velocity components of the receiver as seen from the penetration point are computed and VXI, VYI, and VZI (drift velocity component) are added to obtain VX, VY, and VZ used in the second-order calculations. If this option is other than ORBT, the user specifies VX = VXI, VY = VYI, and VZ = VZI. If VXI = VYI = VZI = 0.0, the program supplies nominal values.

After a set of cards is read and the requested options are executed and the outputs listed, the present value of 11 is examined. If this value is 0, the program attempts to read a new title card; if it is 1, the program attempts to read a new namelist card; and if it is 2, the program terminates.

Table 3

CONTENTS OF CHANGING-PARAMETER(S)/OPTIONS CARD

Column Numbers	Name of Variable	Contents	
		For One Variable	For Two Variables
1-4	NAME	Changing-parameter indicator	Changing-parameter indicators
9-16	A1	Initial value	Initial latitude
17-24	A2	Final value	Initial longitude
25-32	A3	Increment	Final latitude
33-40	A4	--	Final longitude
41-42	NA5	--	Number of increments
		Definition	
43-44	NSCND	Specifies calculation points on which to perform second-order calculations.	
45-48	DLTMMX	Maximum time lag, in seconds.	
49-56	VXI	In ORBT mode, velocity components added to components due to source motion; otherwise, total velocity component used in second-order calculation. Program supplies values if VXI = VYI = VZI = 0.0 (see text).	
57-64	VYI		
65-72	XZI		
73-80	FREQ2	Second frequency (MHz for 2-frequency correlation).	

For model development and testing, a plot routine was used in conjunction with IONSCNT to produce graphs such as those in Figures 5 through 11 of Quarterly Technical Report 7 (Fremouw et al., 1977). The available version of IONSCNT provides arrays that the user can employ with his own computer peripherals. In the absence of user modification, the arrays will be output in tabular form along with identifying information, as shown in the sample calculations below.

B. Sample Calculations

In Figure 6 we show the standard IONSCNT output for a case in which the orbit option was used and two-frequency intensity correlations were requested. The card inputs are shown in Figure 5(a). The title is

F-LAYER PRODUCED VHF-UHF SCINTILLATION

CALCULATED FROM A MODEL DEVELOPED BY STANFORD RESEARCH INSTITUTE,
MENLO PARK, CALIFORNIA.

AARONS, ET. AL. (MOD. TO BE ON ORBIT)

INPUT CONDITIONS USED FOR THIS CALCULATION WERE :

FREQUENCY= 54.00 MHZ SUNSPOT NO.= 47. DAY 31. OUT OF 365 KP INDEX = 1.00 TIME= 6.00 LMT AT RECEIVER FOR FIRST ORBIT POINT

RECEIVER COORDINATES LAT= 42.63 DEG LONG= -70.81 DEG ALT= .200 KM
TRANSMITTER COORDINATES LAT= 17.63 DEG LONG= -70.81 DEG ALT= 940.000 KM

(FOR THIS RUN, THE CHANGING PARAMETERS WERE: TRANSMITTER LATITUDE AND LONGITUDE ALONG ORBIT)

	T-LAT	T-LONG	PSIBP	SGX2	SGY2	CRXY	SGLA2	SGPM2	CRLAPM	S4	PRMS	CIF1F2
1	17.633	-70.840	39.991	.04448	.13157	-.03032	.02099	3.34167	-.10219	.54130	106.956	
2	22.635	-71.002	40.990	.02521	.08879	-.02025	.01010	2.09171	-.05600	.39201	84.668	
3	27.636	-71.149	38.172	.01650	.06898	-.01469	.00474	1.54689	-.03304	.30300	72.855	
4	32.638	-71.276	29.792	.01434	.06995	-.01333	.00257	1.52649	-.02435	.27283	72.400	
5	37.639	-71.375	11.933	.02911	.12840	-.02249	.00270	2.97354	-.03751	.38358	100.658	
6	42.639	-71.436	20.044	.01689	.09722	-.01472	.00130	2.10275	-.02075	.29295	84.971	
7	47.638	-71.444	51.353	.01235	.07354	-.01161	.00135	1.55818	-.01753	.25007	73.176	
8	52.636	-71.378	69.504	.02559	.11359	-.01977	.00401	2.59835	-.03901	.36723	94.389	
9	57.632	-71.202	78.223	.06087	.19440	-.03362	.01129	5.10653	-.09168	.57221	132.204	
10	62.625	-70.854	81.695	.11768	.32453	-.03103	.00395	10.13274	-.07715	.72710	186.500	
11	67.613	-70.218	81.875	.21993	.43904	-.00782	.00011	18.68029	-.01907	.88503	254.325	
	FOR FREQ2= 64.00 MHZ											
1				.02923	.09956	-.02260	.01170	2.38223	-.06437	.42349	90.343	.98824
2				.01639	.06618	-.01454	.00539	1.49092	-.03452	.30593	71.521	.99292
3				.01060	.05103	-.01034	.00249	1.10214	-.02018	.23688	61.532	.99557
4				.00908	.05168	-.00929	.00134	1.08722	-.01484	.21349	61.139	.99656
5				.01820	.09667	-.01620	.00145	2.11738	-.02315	.30191	85.253	.99457
6				.01041	.07224	-.01030	.00068	1.49722	-.01269	.22834	71.754	.99676
7				.00769	.05425	-.00804	.00070	1.10955	-.01068	.19496	61.792	.99734
8				.01613	.08507	-.01418	.00214	1.85052	-.02402	.28813	79.713	.99456
9				.03909	.15018	-.02594	.00637	3.63708	-.05812	.45609	111.611	.98907
10				.07505	.26500	-.02703	.00239	7.21406	-.05067	.40477	157.138	.99092
11				.14648	.38859	-.00892	.00007	13.29876	-.01338	.78621	213.951	.99807

FIGURE 6 SAMPLE OUTPUT FROM IONSCNT SHOWING TWO-FREQUENCY INTENSITY CORRELATION

supplied by the user. The fixed parameters for the run are listed to verify the input conditions. The six sigmas and the intensity and phase scintillation indices are listed for each point together with the Briggs-Parkin angle (the angle between the local magnetic field direction and the propagation vector) and the variable parameters for the run. The points are numbered for reference.

In the second list of numbers the first-order moment for the second frequency is listed together with the two-frequency intensity correlation for intensity, CIF1F2. The two-frequency intensity correlation is described in the Appendix, Section 6.

In Figure 7(a) we show a second example using the orbit option. For this example, however, the second-order moments were requested for every seventh point. The data cards are shown in Figure 5(b). The second-order output is shown in Figure 7(b).

The "effective" velocity VEFF is defined in the Appendix, Section 2. The effective velocity is a function of the true scan velocity and the anisotropy parameters. It accounts for the fact that for the same scan velocity, the time structure of the actual signal is more rapid when the scan is across the principal irregularity axis than when it is along the principal irregularity axis. The azimuth of the scan velocity is the true azimuth of the scan velocity component perpendicular to the line of sight projected onto the receiver plane (tangent to the earth).

The axial ratio and true azimuth of the contours of constant correlation in the receiver plane are also listed. The lag parameter in meters is measured along the scan direction. The listed parameters are shown schematically in Figure 8 for point 8. By comparison with the corresponding parameters for point 1, it can be seen that for point 1 the scan velocity is closer to the direction of the semi-minor axis and the ellipse is more elongated. Thus, the effective scan velocity is larger.

The correlation functions for phase and amplitude are listed under the columns marked COMPOSITE [see, for example, Figures 7(b) and 9(b)]. For reference purposes the separate phase and amplitude correlation

F-LAYER PRODUCED VHF-UHF SCINTILLATION

CALCULATED FROM A MODEL DEVELOPED BY STANFORD RESEARCH INSTITUTE, MENLO PARK, CALIFORNIA.

AURORAL

INPUT CONDITIONS USED FOR THIS CALCULATION WERE :

FREQUENCY= 137.68 MHZ SUNSPOT NO.= 50. DAY 150. OUT OF 365 KP INDEX = 5.00 TIME= 2.38 LMT AT RECEIVER FOR FIRST ORBIT POINT

RECEIVER COORDINATES LAT= 65.13 DEG LONG=-147.49 DEG ALT= .195 KM
TRANSMITTER COORDINATES LAT= 79.40 DEG LONG= -80.30 DEG ALT= 1000.000 KM

(FOR THIS RUN, THE CHANGING PARAMETERS WERE: TRANSMITTER LATITUDE AND LONGITUDE ALONG ORBIT)

	T-LAT	T-LONG	PSIEF	SGX2	SGY2	CRXY	SGLA2	SGPH2	CRLAPH	S4	PRMS
1	79.393	-80.332	76.364	.08105	.30299	-.01199	.00010	8.58406	-.01260	.63479	171.417
2	80.042	-92.056	73.875	.07400	.29792	-.01161	.00008	8.07575	-.01141	.61466	166.241
3	80.249	-104.801	74.875	.06574	.28547	-.01126	.00007	7.53956	-.01001	.58795	160.613
4	79.989	-117.478	73.317	.06003	.27292	-.01094	.00006	7.03069	-.00880	.56415	155.094
5	79.294	-129.035	71.156	.05464	.26193	-.01068	.00005	6.60953	-.00785	.54156	150.380
6	78.243	-138.900	68.366	.05136	.25458	-.01062	.00004	6.34096	-.00727	.52737	147.298
7	76.919	-147.012	64.967	.05114	.25338	-.01095	.00004	6.30576	-.00720	.52592	146.809
8	75.398	-153.553	61.084	.05574	.26164	-.01201	.00005	6.83063	-.00798	.54427	150.620
9	73.735	-158.937	57.024	.06095	.26365	-.01441	.00006	7.54992	-.01049	.59182	160.729
10	71.968	-163.316	53.303	.09681	.32324	-.01894	.00019	9.51395	-.01732	.67748	180.566
11	70.126	-166.951	50.524	.19574	.37619	-.02534	.00059	13.18119	-.03529	.79365	213.111
12	68.228	-170.010	48.081	.22411	.41777	-.02915	.00155	17.82966	-.06522	.88809	248.559
13	66.287	-172.620	48.924	.23995	.42602	-.02899	.00155	19.03881	-.06753	.90183	256.960
14	64.313	-174.879	44.956	.21513	.41441	-.02778	.00086	17.26579	-.04671	.87428	244.520
15	62.313	-176.849	60.801	.19016	.40110	-.02655	.00050	15.53444	-.03596	.84335	231.721
16	60.292	-178.595	61.992	.17034	.38739	-.02549	.00035	14.16632	-.02936	.81521	221.086
17	58.254	179.845	62.647	.15072	.37030	-.02615	.00029	12.78135	-.02557	.78496	209.792
18	56.202	178.438	63.890	.13751	.34501	-.02603	.00026	11.12673	-.02277	.75795	195.525
19	54.140	177.158	64.009	.10111	.31104	-.02662	.00024	[illegible]	-.02017	.67924	177.812
20	52.068	175.965	63.926	.07376	.26954	-.02633	.00023	[illegible]	-.01769	.59872	158.380
21	49.988	174.903	63.436	.05653	.22362	-.02589	.00020	[illegible]	-.01708	.52276	139.765

* INDICATES ACCURACY OF VALUE MAY BE QUESTIONABLE DUE TO POOR INTEGRATION CONVERGENCE

(a) FIRST-ORDER STATISTICS

FIGURE 7 SAMPLE IONSCNT OUTPUT

AURORAL

SECOND-ORDER OUTPUT FOR POINT 1

SCAN
VEFF= 438.46 M/SEC
AZ. OF SCAN= 87.12

DIFFRACTION PATTERN
AXIAL RATIO= 11.07
AZ. OF MAJOR AXIS= 25.95

LAG SEC	LAG M	PHASE AUTOCORRELATION FUNCTION SCATTER	FOCUS	COMPOSITE	INTENSITY AUTOCORRELATION FUNCTION SCATTER	FOCUS	COMPOSITE
0.00	0.00	1.00000	1.00000	1.00000	1.00000	1.00000	1.00000
.30	897.23	.65436	.93741	.99554	.90051	.98885	.99851
.60	1794.45	.87163	.99169	.98515	.74333	.97504	.97334
.90	2691.68	.77639	.98151	.97049	.58890	.74736	.84441
1.20	3588.90	.68515	.95766	.95228	.45450	.60830	.69450
1.50	4486.13	.59694	.95048	.93123	.34555	.48031	.53595
1.80	5383.35	.51611	.93038	.90782	.26037*	.37645	.40386*
2.10	6280.58	.44355	.90776	.88248	.19527*	.30114	.29527*
2.40	7177.80	.37936	.88306	.85563	.14626	.25243	.14626
2.70	8075.03	.32317	.85669	.82764	.10972	.22405	.10973
3.00	8972.26	.27439	.82904	.79883	.08265	.21191	.08248

SECOND-ORDER OUTPUT FOR POINT 8

SCAN
VEFF= 583.93 M/SEC
AZ. OF SCAN= 28.55

DIFFRACTION PATTERN
AXIAL RATIO= 3.53
AZ. OF MAJOR AXIS= 98.17

LAG SEC	LAG M	PHASE AUTOCORRELATION FUNCTION SCATTER	FOCUS	COMPOSITE	INTENSITY AUTOCORRELATION FUNCTION SCATTER	FOCUS	COMPOSITE
0.00	0.00	1.00000	1.00000	1.00000	1.00000	1.00000	1.00000
.30	319.51	.92413	.99069	.99204	.86940	.93938	.86940
.60	639.01	.81013	.98536	.97582	.70470	.78373	.70470
.90	958.52	.68556	.94774	.95237	.54864	.59578	.54864
1.20	1278.03	.56906	.94461	.92381	.43110*	.42815	.43110*
1.50	1597.53	.46736	.91573	.89132	.34282	.30942	.34282
1.80	1917.04	.37992	.88330	.85589	.27623	.24537	.27623
2.10	2236.55	.30667	.84790	.81803	.22467	.21993	.22466
2.40	2556.05	.24615	.81042	.77969	.18419	.21686	.18419
2.70	2875.56	.19668	.77164	.74034	.15127	.22810	.15127
3.00	3195.06	.15655	.73226	.70091	.12422	.23031	.12422

SECOND-ORDER OUTPUT FOR POINT 15

SCAN
VEFF= 765.78 M/SEC
AZ. OF SCAN= 71.06

DIFFRACTION PATTERN
AXIAL RATIO= 2.53
AZ. OF MAJOR AXIS=-79.05

LAG SEC	LAG M	PHASE AUTOCORRELATION FUNCTION SCATTER	FOCUS	COMPOSITE	INTENSITY AUTOCORRELATION FUNCTION SCATTER	FOCUS	COMPOSITE
0.00	0.00	1.00000	1.00000	1.00000	1.00000	1.00000	1.00000
.30	545.08	.89016	.99331	.99705	.74124	.94294	.74127
.60	1090.15	.72343	.97383	.99260	.48163	.67445	.48167
.90	1635.23	.56546	.94421	.92284	.29491	.52076	.28495
1.20	2180.30	.43203	.90369	.87900	.18290	.44548	.18295
1.50	2725.38	.32511	.85765	.82859	.12267	.45741	.12219
1.80	3270.45	.24202	.80750	.77671	.09530	.49383	.09541
2.10	3815.53	.17869	.75506	.72367	.08063	.52257	.08076
2.40	4360.60	.13110	.70193	.67085	.06362	.53094	.06375
2.70	4905.68	.09506	.64933	.61918	.03154	.51692	.03168
3.00	5450.75	.06954	.59814	.56938	.02265	.46830	.02299

(b) SECOND-ORDER STATISTICS

FIGURE 7 (Concluded)

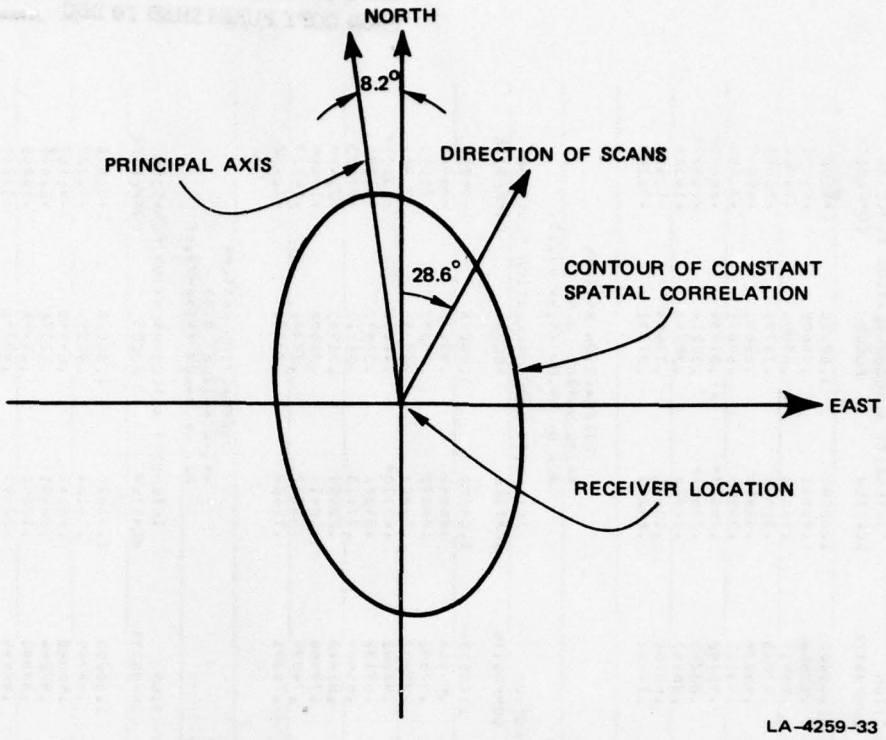

FIGURE 8 DIAGRAM SHOWING RELATIVE ORIENTATION OF SCAN VELOCITY AND CONTOUR OF CONSTANT SPATIAL AUTOCORRELATION

functions for the scatter and focus components are also listed. To reiterate, the lag parameter in meters is a measure of the correlation distance along the direction of scan.

As a final example, in Figures 9(a) and 9(b) we show the outputs for a run with the source and receiver fixed and frequency varying from 50 to 500 MHz in steps of 50 MHz with second-order outputs requested for every fourth point. The corresponding input cards are shown in Figure 5(c).

The user is warned that the full second-order outputs require considerable computation. Thus, they are time consuming and therefore expensive to generate. The first example presented in this section used 143 s of CDC 6400 computer time including the generation of plots not shown here. By comparison, the second example used ~ 400 s of CDC 6400 computer time.

F-LAYER PRODUCED VHF-UHF SCINTILLATION

CALCULATED FROM A MODEL DEVELOPED BY STANFORD RESEARCH INSTITUTE, MENLO PARK, CALIFORNIA.

ANCON FREQUENCY

INPUT CONDITIONS USED FOR THIS CALCULATION WERE :

FREQUENCY= 50.00 MHZ SUNSPOT NO.= 100. DAY 290. OUT OF 365 KP INDEX = 5.00 TIME= 22.50 LMT AT RECEIVER

RECEIVER COORDINATES LAT= -11.78 DEG LONG= -77.15 DEG ALT= .049 KM
TRANSMITTER COORDINATES LAT= 0.00 DEG LONG=-110.00 DEG ALT= 35800.000 KM

(FOR THIS RUN, THE CHANGING PARAMETER WAS: FREQUENCY)

	FREQ	PSIBP	SGX2	SGY2	CRXY	SGLA2	SGPH2	CRLAPH	S4	PRMS
1	50.000	98.228	.49058	.49706	-.00272	.00210	76.27420	-.15179	1.00829	509.807
2	100.000	98.228	.27574	.39078	-.05018	.05669	19.01238	-.39410	1.14129	257.185
3	150.000	98.228	.12807	.25812	-.05179	.09503	8.38011	-.34017	1.08669	169.712
4	200.000	98.228	.06681	.17327	-.03823	.06906	4.69823	-.21746	.82727	126.826
5	250.000	98.228	.03900	.12213	-.02717	.03834	3.01271	-.12964	.60006	101.563
6	300.000	98.228	.02475	.09012	-.01963	.02109	2.09770	-.08013	.45172	84.804
7	350.000	98.228	.01672	.06903	-.01456	.01217	1.54449	-.05216	.35432	72.804
8	400.000	98.228	.01185	.05449	-.01108	.00741	1.18441	-.03561	.28731	63.781
9	450.000	98.228	.00871	.04407	-.00864	.00473	.93695	-.02530	.23910	56.750
10	500.000	98.228	.00660	.03637	-.00687	.00315	.75961	-.01859	.20310	51.115

* INDICATES ACCURACY OF VALUE MAY BE QUESTIONABLE DUE TO POOR INTEGRATION CONVERGENCE

(a) FIRST-ORDER STATISTICS

FIGURE 9 SAMPLE IONSCNT OUTPUT WITH VARYING FREQUENCY

ANCON FREQUENCY

SECOND-ORDER OUTPUT FOR POINT 1

SCAN
VEFF= 40.64 M/SEC
AZ. OF SCAN=100.03

DIFFRACTION PATTERN
AXIAL RATIO= 23.57
AZ. OF MAJOR AXIS= -.20

LAG SEC	LAG M	PHASE AUTOCORRELATION FUNCTION SCATTER	FOCUS	COMPOSITE	INTENSITY AUTOCORRELATION FUNCTION SCATTER	FOCUS	COMPOSITE
0.00	0.00	1.00000	1.00000	1.00000	1.00000	1.00000	1.00000
6.00	319.60	.56734	.94366	.92317	.02211	1.00000	.03023
12.00	639.20	.24388	.80882	.77805	.00105	1.00000	.00935
18.00	958.79	.09685	.65132	.62113	.00010	1.00000	.00641
24.00	1278.39	.03698	.50463	.47917	-.00005	1.00000	.00826
30.00	1597.99	.01379	.38133	.36132	-.00008	1.00000	.00822
36.00	1917.59	.00506	.28326	.26811	-.00009	1.00000	.00822
42.00	2237.18	.00184	.20782	.19661	-.00008	1.00000	.00823
48.00	2556.78	.00066	.15106	.14287	-.00006	.99999	.00825
54.00	2876.38	.00024	.10902	.10309	-.00002	.99946	.00828
60.00	3195.98	.00008	.07822	.07396	.00002	.99327	.00827

SECOND-ORDER OUTPUT FOR POINT 5

SCAN
VEFF= 40.64 M/SEC
AZ. OF SCAN=100.03

DIFFRACTION PATTERN
AXIAL RATIO= 23.57
AZ. OF MAJOR AXIS= -.20

LAG SEC	LAG M	PHASE AUTOCORRELATION FUNCTION SCATTER	FOCUS	COMPOSITE	INTENSITY AUTOCORRELATION FUNCTION SCATTER	FOCUS	COMPOSITE
0.00	0.00	1.00000	1.00000	1.00000	1.00000	1.00000	1.00000
6.00	319.60	.56734	.94366	.92317	.22482	.41489	.30222
12.00	639.20	.24388	.80882	.77805	-.25294	.27795	.00545
18.00	958.79	.09685	.65132	.62113	-.37470	.33596	-.02849
24.00	1278.39	.03698	.50463	.47917	-.16528	.26681	.05186
30.00	1597.99	.01379	.38133	.36132	.08106	.20808	.13460
36.00	1917.59	.00506	.28326	.26811	.07806	.14169	.10221
42.00	2237.18	.00184	.20782	.19661	-.03431	.09430	.02728
48.00	2556.78	.00066	.15106	.14287	-.01613	.06240	.02118
54.00	2876.38	.00024	.10902	.10309	.03645	.04135	.03602
60.00	3195.98	.00008	.07822	.07396	-.03244*	.02752	-.00242*

SECOND-ORDER OUTPUT FOR POINT 9

SCAN
VEFF= 40.64 M/SEC
AZ. OF SCAN=100.03

DIFFRACTION PATTERN
AXIAL RATIO= 23.57
AZ. OF MAJOR AXIS= -.20

LAG SEC	LAG M	PHASE AUTOCORRELATION FUNCTION SCATTER	FOCUS	COMPOSITE	INTENSITY AUTOCORRELATION FUNCTION SCATTER	FOCUS	COMPOSITE
0.00	0.00	1.00000	1.00000	1.00000	1.00000	1.00000	1.00000
6.00	319.60	.56734	.94366	.92317	-.03280	.39718	.11118
12.00	639.20	.24388	.80882	.77805	-.61514	.26371	-.31571
18.00	958.79	.09685	.65132	.62113	-.34479	.31994	-.11966
24.00	1278.39	.03698	.50463	.47917	.06899	.27227	.13632
30.00	1597.99	.01379	.38133	.36132	-.04230	.19655	.03797
36.00	1917.59	.00506	.28326	.26811	-.03498	.13329	.02165
42.00	2237.18	.00184	.20782	.19661	.00090*	.08846	.03016*
48.00	2556.78	.00066	.15106	.14287	-.06292*	.05842	-.02162*
54.00	2876.38	.00024	.10902	.10309	.01329*	.03667	.02161*
60.00	3195.98	.00008	.07822	.07396	.02970*	.02571	.02801*

(b) SECOND-ORDER STATISTICS

FIGURE 9 (Concluded)

IV THE AUXILIARY STATISTICS PROGRAM DIST

A. General

Program DIST is to be used in conjunction with Program IONSCNT to provide the user with detailed fading statistics for a signal that has passed through the ionosphere. The necessary input parameters for DIST are computed in Program IONSCNT as described in Sections II and III. Program DIST provides the user with statistical information about the received signal in the form of probability density functions for amplitude and phase (tables and plots). The user can estimate fading statistics from the cumulative probability density functions for amplitude. A cumulative probability density function of phase is also provided.

B. Description of the Program

Program DIST computes the density distribution of phase and amplitude for the two-component model of scintillation statistics. The two-component model can be characterized as the product of two statistically independent components having, respectively, Gaussian and log-normal statistics as described in Quarterly Technical Report 7 (Fremouw et al., 1977). The joint probability density function (PDF) of amplitude, a, and phase, ϕ, is given by the two-dimensional integral

$$P_{A\Phi}(a,\phi) = \frac{1}{A}\int_{-\infty}^{\infty}\int_{-\infty}^{\infty} e^{2\chi_s} P_{x_s y_s}\left[\left(e^{\chi_s}\cos\phi_s - \eta\right), e^{\chi_s}\sin\phi_s\right] \tag{1}$$

$$P_{\chi_f\phi_f}\left[\left(\ln(a) + \sigma_{\chi_f}^2 - \chi_s\right), \left(\phi - \phi_s\right)\right] d\chi_s d\phi_s$$

In Eq. (1), $P_{x_s y_s}(.,.)$ is the joint PDF for the real and imaginary parts of the scatter component, while $P_{\chi_f \phi_f}(.,.)$ is the joint PDF for the log-amplitude and phase of the focus component, Both PDFs are assumed to have the general joint Gaussian form. Thus, they are specified in terms of the six sigmas, σ_x^2, σ_y^2, σ_{xy}, $\sigma_{\chi_f}^2$, σ_ϕ^2, and $\sigma_{\chi\phi}$, which are variances and covariances of the respective components. These parameters are input to this program and are given by Program IONSCNT as: σ_x^2 = SGX2; σ_y^2 = SGY2; σ_{xy} = CRXY; $\sigma_{\chi_f}^2$ = SGLA2; $\sigma_{\phi_f}^2$ = SGPH2; $\sigma_{\chi\phi}$ = CRLAPH. The mean values of x and y for the scatter component and χ and ϕ for the focus component are, respectively, $\eta_\chi^2 = 1 - \sigma_x^2 - \sigma_y^2$ and 0; and $\ell n(a) + \sigma_{\chi_f}^2$ and 0. These mean values ensure energy conservation for the composite signal and the scatter and focus components separately.

The user is generally interested in the statistics of amplitude and phase separately. Thus, we integrate Eq. (1) over the phase variable to obtain the PDF for amplitude, $P_A(a)$, which can be written as

$$P_A(a) = a^{-1} \int_{-\infty}^{\infty} e^{\chi_s} P_{A_s}\left(e^{\chi_s}\right) P_{\chi_f}\left(\ell n(a) + \sigma_{\chi_f}^2 - \chi_s\right) d\chi_s \qquad (2)$$

In Eq. (2), $P_{A_s}(\cdot)$ is the amplitude PDF for the scatter component and $p_{\chi_f}(\cdot)$ is the log amplitude PDF for the focus component.

A similar calculation gives the PDF for phase:

$$P_\phi(\phi) = \int_{-\infty}^{\infty} P_{\phi_s}\left(\phi_s\right) P_{\phi_f}\left(\phi - \phi_s\right) d\phi_s \quad . \qquad (3)$$

In Eq. (3), $P_{\phi_s}(\cdot)$ is the phase PDF for the scatter component--the Hatfield distribution (Hatfield and Rino. 1975--and $P_{\phi_f}(\cdot)$ is the phase PDF for the focus component.

In addition to the above three distributions, PDFs $P_A(a)$ and $P_\phi(\phi)$, the corresponding cumulative density functions (CDF), are computed. For the amplitude, the CDF is presented in dB for fade-margin computations. The output represents the probability of fading below a specified amplitude. The CDF of phase represents the probability of a phase change greater than a specified value. (Both positive and negative changes are considered.) The inputs to DIST are generated by IONSCNT.

Table 4 gives a list of the subroutines required, together with a brief description of the function of each routine. The operation of DIST is straightforward. The various functions are evaluated to generate the necessary integrands, which are then evaluated by numerical integration.

Table 4

SUBROUTINES USED IN PROGRAM DIST

Subroutine	Function	Reference
DIST	Control program, reads input; calls subroutines.	
CDFP	Computes; lists; plots CDF of Eq. (3).	DIST
CPFI	Computes; lists; plots CDF of Eq. (2).	DIST
COMP2A	Computes Eq. (2).	DIST
FEHLIN	Computes error function complement.	PRTHET
FMAX	Used to compute limits of integration for Eq. (2).	PNEW
GAUSS	Computes one-dimensional Gaussian density function.	PGTHET PAAMP
GAU2ZM	Computes bivariate Gaussian zero mean density function.	PRAPH
GRAPH4	System-dependent plotting routine. User may substitute his own or a dummy routine.	CDFP CPFI PDFP PDFI
ITERAT	Finds zero of a function by iteration.	PNEW
NUPHAS	Computes $p_\phi(\cdot)$ and stores in array.	DIST
PAAMP	Computes integrand of Eq. (2).	PNEW
PDFI	Lists and plots Eq. (2).	DIST

Table 4 (Concluded)

Subroutine	Function	Reference
PDFP	Lists and plots Eq. (3).	DIST
PGTHET	Computes integrand of Eq. (3).	NUPHAS
PNEW	Computes $P_A(\cdot)$ and stores in array.	COMP2A
PR	Computes $P_{A_s}(\cdot)$.	PAAMP
PRAPH	Computes integrand needed to find $P_{A_s}(\cdot)$.	PR
PRTHET	Computes $p_{\phi_s}(\cdot)$	PGTHET
QG5	Five-point Gaussian quadrature.	PNEW
QG6	Six-point Gaussian quadrature.	PR
QG6L2	Six-point Gaussian quadrature in two parts	PNEW
QG16	Sixteen-point Gaussian quadrature.	PR
QG20	Twenty-point Gaussian quadrature.	NUPAAS
SYGN	Return plus or minus one, depending on sign of argument.	ITERAT

C. Instructions for Use

1. Input

The input required for this program is one card per data set. The card contains the six parameters of the two-component distribution which are obtained from the output of IONSCNT. The parameters are SGX2, SGY2, CRXY, SGLA2, SGPH2, and CRLAPH. They must be written with a decimal point in ten-column fields. A blank card indicates the end of all data sets.

The user must substitute his own plotting subroutine for GRAPH4 if he desires plots. If listings only are desired a dummy subroutine GRAPH4(...) may be supplied.

2. Output

The output consists of tables and plots of four distributions:

- P(A), the amplitude probability density versus amplitude normalized to the undisturbed amplitude.
- CPF, the cumulative amplitude probability versus signal strength in dB relative to the undisturbed level.
- P(PHI) the phase probability density versus phase angle in radians.
- Probability of phase change greater than THETA in radians.

3. Examples

We present two examples to illustrate the use of DIST. The card inputs for both examples are shown in Figure 10. In the first example (Figure 11), very large phase changes occur, so the cumulative phase density is not meaningful and therefore is not computed. In the second example (Figure 12), all four distributions are shown. The data output format is self-explanatory. The running time on the CDC 6400 for the two examples was 29.2 sec. This time includes computation, plotting, and listing.

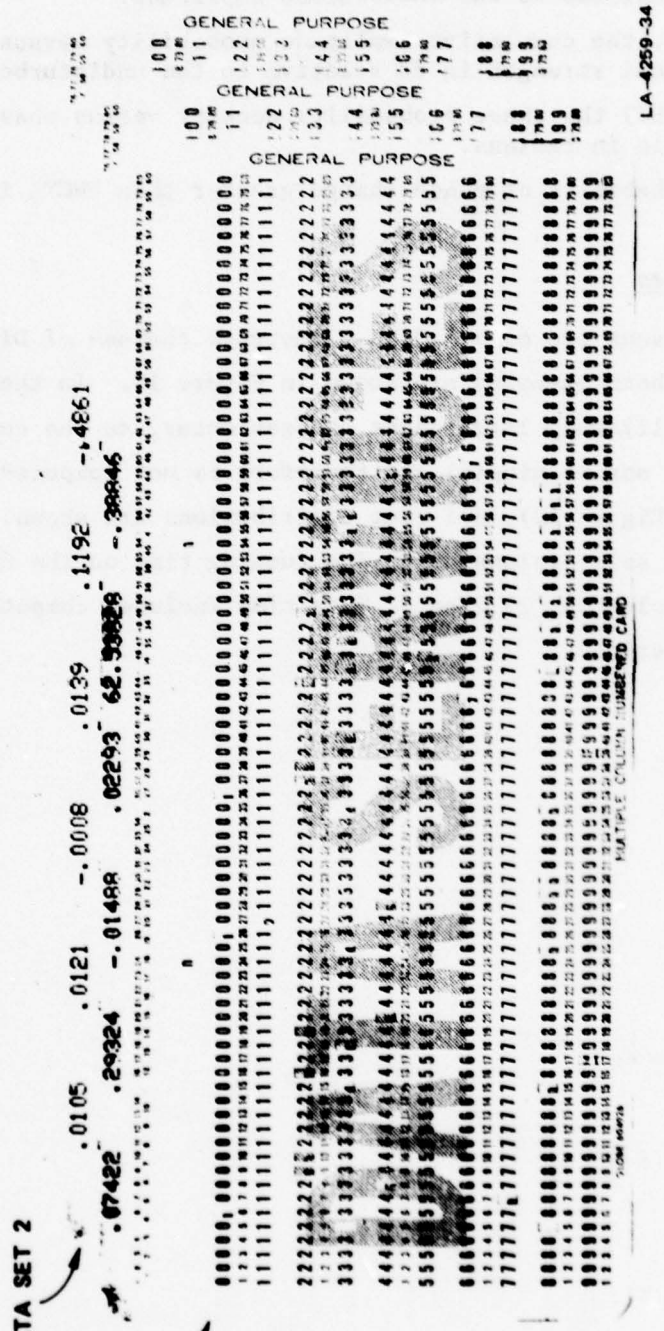

FIGURE 10 SAMPLE CARD INPUT FOR DIST

PARAMETERS FOR THE TWO-COMPONENT SCINTILLATION MODEL

SGX2= .07422 SGY2= .29324 CRXY= -.01488 SGLA2= .02293 SGPH2= 62.53828 CRLAPH= -.38846

PROBABILITY DENSITY, P(A), VS. AMPLITUDE/UNDISTURBED AMPLITUDE

SGX2= .074 SGY2= .29 CRXY= -.015 SGLA2= .023 SGPH2= 62.54 CRLAPH= -.39

A	P(A)	A	P(A)	A	P(A)	A	P(A)	A	P(A)	A	P(A)	A	P(A)	A	P(A)
.00	.000	.05	.005	.10	.013	.15	.026	.20	.047	.25	.080	.30	.130	.35	.200
.40	.291	.45	.404	.50	.536	.55	.679	.60	.826	.65	.965	.70	1.087	.75	1.182
.80	1.244	.85	1.271	.90	1.263	.95	1.223	1.00	1.157	1.05	1.071	1.10	.972	1.15	.867
1.20	.760	1.25	.657	1.30	.560	1.35	.471	1.40	.392	1.45	.323	1.50	.264	1.55	.214
1.60	.172	1.65	.138	1.70	.109	1.75	.086	1.80	.068	1.85	.053	1.90	.041	1.95	.032
2.00	.025	2.05	.019	2.10	.015	2.15	.011	2.20	.009	2.25	.006	2.30	.005	2.35	.004
2.40	.003	2.45	.002	2.50	.002	2.55	.001	2.60	.001	2.65	.001	2.70	.000	2.75	.000
2.80	.000	2.85	.000	2.90	.000	2.95	.000								

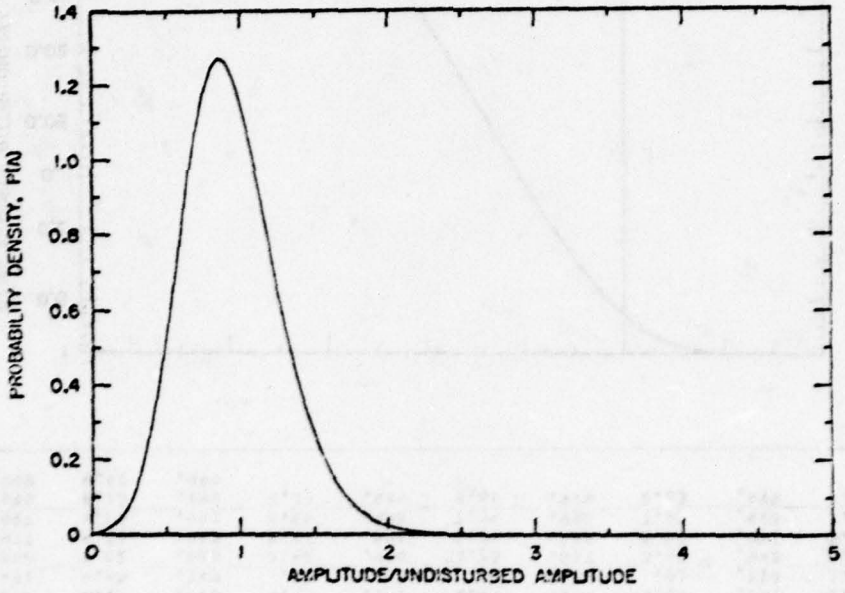

SGX2= .074 SGY2= .29 CRXY= -.015 SGLA2= .023 SGPH2= 62.54 CRLAPH= -.39

(a) AMPLITUDE PROBABILITY DENSITY

FIGURE 11 SAMPLE OUTPUTS FROM DIST FOR HIGH LEVEL OF ACTIVITY

CUMULATIVE PROBABILITY, CPF, VS. SIGNAL STRENGTH IN DB RELATIVE TO UNDISTURBED LEVEL

SGX2= .074 SGY2= .29 CRXY= -.015 SGLA2= .023 SGPH2= 62.54 CRLAPH= -.39

DB	CPF	DB	CPF	DB	CPF	DB	CPF	DB	CPF	DB	CPF	DB	CPF	DB	CPF
-26.02	.000	-20.00	.001	-16.48	.002	-13.98	.003	-12.04	.006	-10.46	.012	-9.12	.020	-7.96	.032
-6.94	.049	-6.02	.073	-5.19	.103	-4.44	.141	-3.74	.186	-3.10	.237	-2.50	.294	-1.94	.355
-1.41	.418	-.92	.481	-.45	.543	.00	.603	.42	.659	.83	.710	1.21	.756	1.58	.796
1.94	.832	2.28	.862	2.61	.888	2.92	.910	3.23	.927	3.52	.942	3.81	.954	4.08	.964
4.35	.971	4.61	.977	4.86	.982	5.11	.986	5.34	.989	5.58	.991	5.80	.993	6.02	.995
6.24	.996	6.44	.997	6.65	.997	6.85	.998	7.04	.998	7.23	.998	7.42	.999	7.60	.999
7.78	.999	7.96	.999	8.13	.999	8.30	.999	8.46	.999	8.63	.999	8.79	.999	8.94	.999
9.10	.999	9.25	.999	9.40	.999										

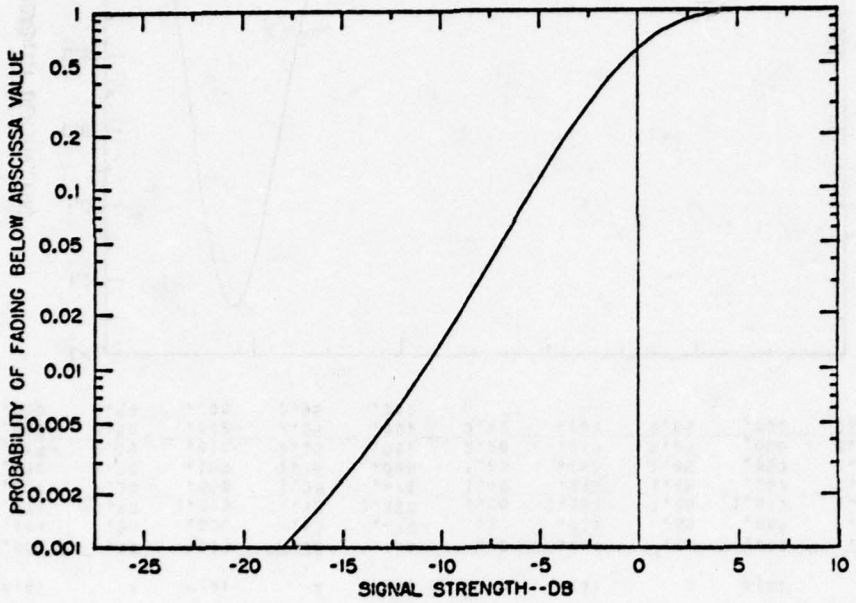

SGX2= .074 SGY2= .29 CRXY= -.015 SGLA2= .023 SGPH2= 62.54 CRLAPH= -.39

(b) CUMULATIVE AMPLITUDE PROBABILITY DENSITY IN dB

FIGURE 11 (Continued)

PROBABILITY DENSITY, P(PHI), VS. PHASE ANGLE IN RADIANS

SGX2= .074 SGY2= .29 CRXY= -.015 SGLA2= .023 SGPH2= 62.54 CRLAPH= -.39

PHI	P(PHI)	PHI	P(PHI)	PHI	P(PHI)	PHI	P(PHI)	PHI	P(PHI)	PHI	P(PHI)	PHI	P(PHI)	PHI	P(PHI)
-5.00	.0412	-4.90	.0415	-4.80	.0418	-4.70	.0421	-4.60	.0425	-4.50	.0428	-4.40	.0431	-4.30	.0434
-4.20	.0437	-4.10	.0440	-4.00	.0442	-3.90	.0445	-3.80	.0448	-3.70	.0451	-3.60	.0453	-3.50	.0456
-3.40	.0458	-3.30	.0461	-3.20	.0463	-3.10	.0466	-3.00	.0468	-2.90	.0470	-2.80	.0472	-2.70	.0474
-2.60	.0476	-2.50	.0478	-2.40	.0480	-2.30	.0482	-2.20	.0484	-2.10	.0485	-2.00	.0487	-1.90	.0488
-1.80	.0490	-1.70	.0491	-1.60	.0493	-1.50	.0494	-1.40	.0495	-1.30	.0496	-1.20	.0497	-1.10	.0498
-1.00	.0499	-.90	.0499	-.80	.0500	-.70	.0501	-.60	.0501	-.50	.0502	-.40	.0502	-.30	.0502
-.20	.0503	-.10	.0503	-.00	.0503	.10	.0503	.20	.0503	.30	.0502	.40	.0502	.50	.0502
.60	.0501	.70	.0501	.80	.0500	.90	.0500	1.00	.0499	1.10	.0498	1.20	.0497	1.30	.0496
1.40	.0495	1.50	.0494	1.60	.0493	1.70	.0492	1.80	.0490	1.90	.0489	2.00	.0487	2.10	.0486
2.20	.0484	2.30	.0482	2.40	.0481	2.50	.0479	2.60	.0477	2.70	.0475	2.80	.0473	2.90	.0471
3.00	.0468	3.10	.0466	3.20	.0464	3.30	.0461	3.40	.0459	3.50	.0456	3.60	.0454	3.70	.0451
3.80	.0449	3.90	.0446	4.00	.0443	4.10	.0440	4.20	.0437	4.30	.0434	4.40	.0431	4.50	.0428
4.60	.0425	4.70	.0422	4.80	.0419	4.90	.0416	5.00	.0413						

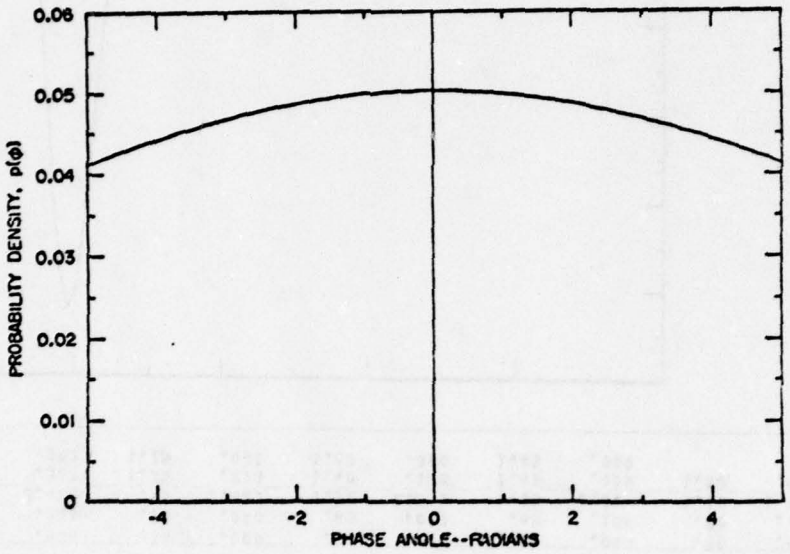

SGX2= .074 SGY2= .29 CRXY= -.015 SGLA2= .023 SGPH2= 62.54 CRLAPH= -.39

SIGNIFICANT PHASE CHANGE GREATER THAN 5 RADIANS--CUMULATIVE PHASE PLOT WILL NOT BE MADE

(c) PHASE PROBABILITY DENSITY

FIGURE 11 (Concluded)

PARAMETERS FOR THE TWO-COMPONENT SCINTILLATION MODEL

SGX2= .01050 SGY2= .01210 CRXY= -.00080 SGLA2= .01390 SGPH2= .11920 CRLAPH= -.48610

PROBABILITY DENSITY, P(A), VS. AMPLITUDE/UNDISTURBED AMPLITUDE

SGX2= .011 SGY2= .01 CRXY= -.001 SGLA2= .014 SGPH2= .12 CRLAPH= -.49

A	P(A)	A	P(A)	A	P(A)	A	P(A)	A	P(A)	A	P(A)	A	P(A)	A	P(A)
.00	0.000	.05	.000	.10	.000	.15	.000	.20	.000	.25	.000	.30	.000	.35	.000
.40	.000	.45	.000	.50	.001	.55	.010	.60	.047	.65	.158	.70	.403	.75	.822
.80	1.384	.85	1.970	.90	2.423	.95	2.621	1.00	2.533	1.05	2.214	1.10	1.772	1.15	1.311
1.20	.906	1.25	.589	1.30	.362	1.35	.213	1.40	.120	1.45	.065	1.50	.034	1.55	.017
1.60	.008	1.65	.004	1.70	.002	1.75	.001	1.80	.000	1.85	.000				

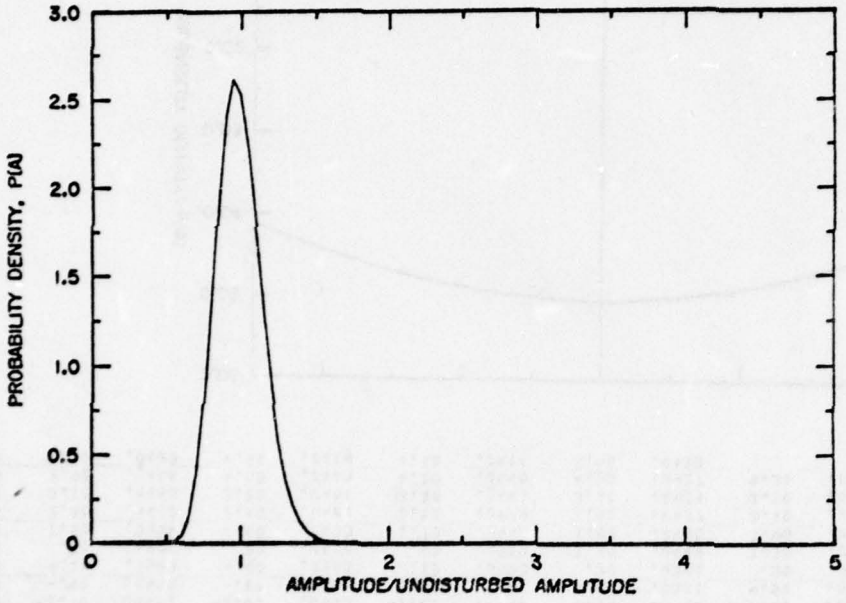

SGX2= .011 SGY2= .01 CRXY= -.001 SGLA2= .014 SGPH2= .12 CRLAPH= -.49

(a) AMPLITUDE PROBABILITY DENSITY

FIGURE 12 SAMPLE OUTPUTS FROM DIST FOR LOW LEVEL OF ACTIVITY

CUMULATIVE PROBABILITY, CPF, VS. SIGNAL STRENGTH IN DB RELATIVE TO UNDISTURBED LEVEL

SGX2= .011 SGY2= .01 CRXY= -.001 SGLA2= .014 SGPH2= .12 CRLAPH= -.49

DB	CPF	DB	CPF	DB	CPF	DB	CPF	DB	CPF	DB	CPF	DB	CPF	DB	CPF
-26.02	-.000	-20.00	.000	-16.48	-.000	-13.98	-.000	-12.04	-.000	-10.46	-.000	-9.12	-.000	-7.96	-.000
-6.94	-.000	-6.02	.000	-5.19	.000	-4.44	.001	-3.74	.006	-3.10	.020	-2.50	.049	-1.94	.104
-1.41	.188	-.92	.299	-.45	.426	.00	.556	.42	.676	.83	.775	1.21	.852	1.58	.908
1.94	.945	2.28	.968	2.61	.982	2.92	.990	3.23	.995	3.52	.997	3.81	.998	4.08	.999
4.35	.999	4.61	.999	4.86	.999	5.11	.999	5.34	.999						

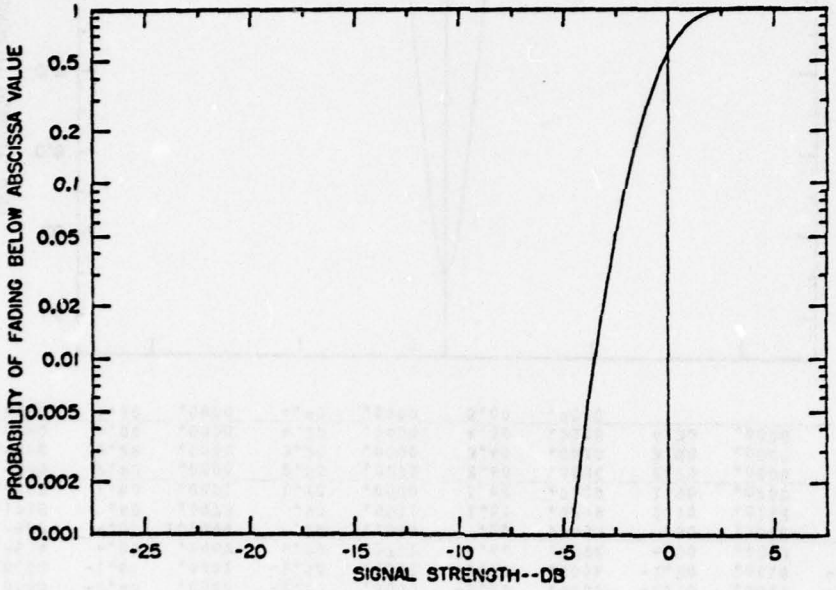

SGX2= .011 SGY2= .01 CRXY= -.001 SGLA2= .014 SGPH2= .12 CRLAPH= -.49

(b) CUMULATIVE AMPLITUDE PROBABILITY DENSITY IN dB

FIGURE 12 (Continued)

PROBABILITY DENSITY, P(PHI), VS. PHASE ANGLE IN RADIANS

SGX2= .011 SGY2= .01 CRXY= -.001 SGLA2= .014 SGPH2= .12 CRLAPH= -.49

PHI	P(PHI)	PHI	P(PHI)	PHI	P(PHI)	PHI	P(PHI)	PHI	P(PHI)	PHI	P(PHI)	PHI	P(PHI)	PHI	P(PHI)
-5.00	.0000	-4.90	.0000	-4.80	.0000	-4.70	.0000	-4.60	.0000	-4.50	.0000	-4.40	.0000	-4.30	.0000
-4.20	.0000	-4.10	.0000	-4.00	.0000	-3.90	.0000	-3.80	.0000	-3.70	.0000	-3.60	.0000	-3.50	.0000
-3.40	.0000	-3.30	.0000	-3.20	.0000	-3.10	.0000	-3.00	.0000	-2.90	.0000	-2.80	.0000	-2.70	.0000
-2.60	.0000	-2.50	.0000	-2.40	.0000	-2.30	.0000	-2.20	.0000	-2.10	.0000	-2.00	.0000	-1.90	.0000
-1.80	.0000	-1.70	.0000	-1.60	.0001	-1.50	.0002	-1.40	.0006	-1.30	.0018	-1.20	.0046	-1.10	.0110
-1.00	.0244	-.90	.0504	-.80	.0962	-.70	.1702	-.60	.2792	-.50	.4243	-.40	.5975	-.30	.7800
-.20	.9436	-.10	1.0580	-.00	1.0994	.10	1.0589	.20	.9453	.30	.7822	.40	.6000	.50	.4266
.60	.2811	.70	.1718	.80	.0973	.90	.0511	1.00	.0249	1.10	.0112	1.20	.0047	1.30	.0018
1.40	.0007	1.50	.0002	1.60	.0001	1.70	.0000	1.80	.0000	1.90	.0000	2.00	.0000	2.10	.0000
2.20	.0000	2.30	.0000	2.40	.0000	2.50	.0000	2.60	.0000	2.70	.0000	2.80	.0000	2.90	.0000
3.00	.0000	3.10	.0000	3.20	.0000	3.30	.0000	3.40	.0000	3.50	.0000	3.60	.0000	3.70	.0000
3.80	.0000	3.90	.0000	4.00	.0000	4.10	.0000	4.20	.0000	4.30	.0000	4.40	.0000	4.50	.0000
4.60	.0000	4.70	.0000	4.80	.0000	4.90	.0000	5.00	.0000						

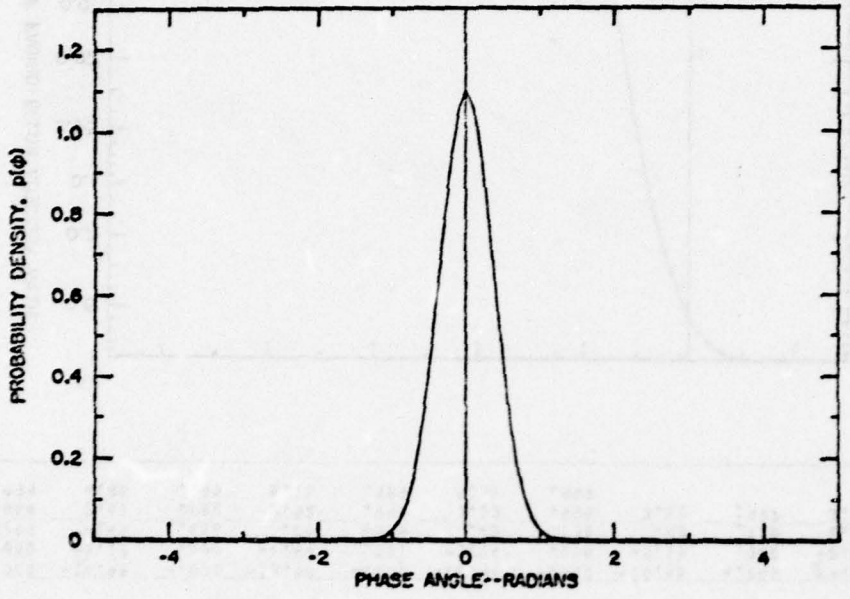

SGX2= .011 SGY2= .01 CRXY= -.001 SGLA2= .014 SGPH2= .12 CRLAPH= -.49

(c) PHASE PROBABILITY DENSITY

FIGURE 12 (Continued)

PROBABILITY OF PHASE CHANGE GREATER THAN THETA IN RADIANS

SGX2= .011 SGY2= .01 CRXY= -.001 SGLA2= .014 SGPH2= .12 CRLAPH= -.49

THETA	PROB	THETA	PROB	THETA	PROB	THETA	PROB	THETA	PROB	THETA	PROB	THETA	PROB	THETA	PROB
4.90	-.000	4.80	.000	4.70	.000	4.60	.000	4.50	.000	4.40	.000	4.30	.000	4.20	.000
4.10	.000	4.00	.000	3.90	.000	3.80	.000	3.70	.000	3.60	.000	3.50	.000	3.40	.000
3.30	.000	3.20	.000	3.10	.000	3.00	.000	2.90	.000	2.80	.000	2.70	.000	2.60	.000
2.50	.000	2.40	.000	2.30	.000	2.20	.000	2.10	.000	2.00	.000	1.90	.000	1.80	.000
1.70	.000	1.60	.000	1.50	.000	1.40	.000	1.30	.000	1.20	.001	1.10	.002	1.00	.006
.90	.013	.80	.027	.70	.054	.60	.098	.50	.168	.40	.270	.30	.408	.20	.582
.10	.783	.00	1.000	-.10	1.000										

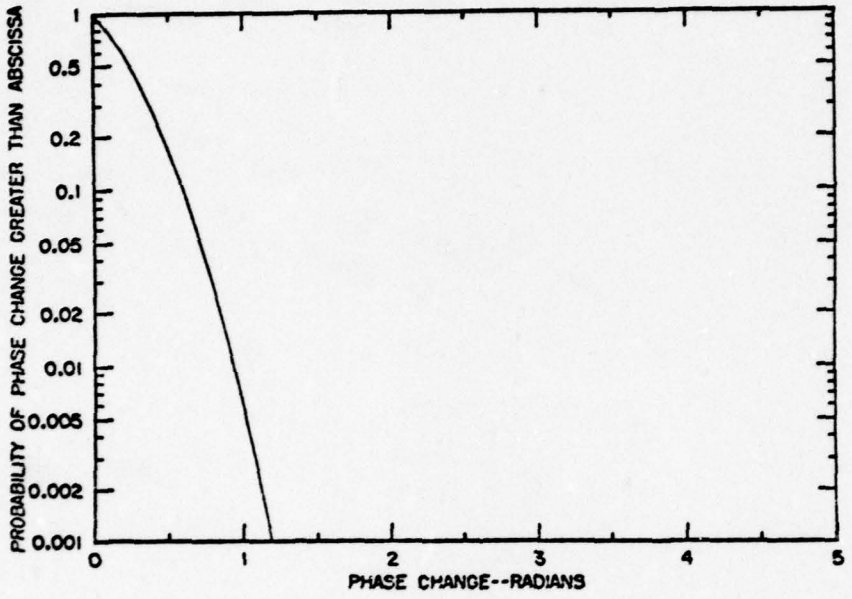

SGX2= .011 SGY2= .01 CRXY= -.001 SGLA2= .014 SGPH2= .12 CRLAPH= -.49

(d) CUMULATIVE PHASE DENSITY

FIGURE 12 (Concluded)

Appendix

SUMMARY OF THEORETICAL CALCULATIONS USED IN IONSCNT

Appendix

SUMMARY OF THEORETICAL CALCULATIONS USED IN IONSCNT

1. Phase Autocorrelation Function

The phase autocorrelation used in IONSCNT is described in Rino and Fremouw (1977). It has the general form

$$R_{\phi}(\vec{\Delta\rho}) = \sigma^2 \, \Delta L \, R\left(f(\vec{\Delta\rho}_s)\right) \tag{A-1}$$

where

$$\vec{\Delta\rho}_s = \vec{\Delta\rho} - \tan\theta \, \hat{a}_{k_T} \, \Delta z \tag{A-2}$$

$$f(\vec{\Delta\rho}_s) = \left[\frac{C\,\Delta\rho_{x_s}^2 - B\,\Delta\rho_{x_s}\,\Delta\rho_{y_s} + A\,\Delta\rho_{y_s}^2}{\left(AC - B^2/4\right)}\right]^{1/2}$$

$$\sigma^2 = r_e^2 \lambda^2 \left(\frac{\langle ab\,\Delta N_e^2\rangle}{\sqrt{AC - B^2/4}\,\cos\theta}\right) \sec\theta\,\kappa \,. \tag{A-4}$$

For $R(y)$ and κ we have used

$$R(y) = \sqrt{1 + \frac{y^2}{2\beta^2}}^{(\gamma - 1/2)} \frac{K_{\gamma-1/2}\left(2\beta/\alpha \sqrt{1 + y^2/2\beta^2}\right)}{K_{\gamma-1/2}(2\beta/2)} \tag{A-5}$$

and

$$\kappa = \sqrt{4\pi\alpha\beta}\, K_{\gamma-1/2}(2\beta/\alpha)/K_{\gamma-1}(2\beta/\alpha) \quad . \tag{A-6}$$

The anisotropy of the irregularities manifests itself in the A, B, C coefficients. These coefficients are given in terms of the elongation parameters along and transverse to the field (a and b, respectively), the orientation angle of the transverse axis, δ, the magnetic dip angle, ψ, and the propagation angles θ and φ, as follows:

$$A = \left[\hat{C}_{11} + \hat{C}_{33} \tan^2\theta \cos^2\varphi - 2\hat{C}_{13} \tan\theta \cos\varphi\right] \tag{A-6a}$$

$$B = 2\left[\hat{C}_{12} + \hat{C}_{33} \tan^2\theta \sin\varphi \cos\varphi - \tan\theta \left(\hat{C}_{13} \sin\varphi \right.\right. \tag{A-6b}$$

$$\left.\left. + \hat{C}_{23} \cos\varphi\right)\right] \tag{A-6b}$$

$$C = \left[\hat{C}_{22} + \hat{C}_{33} \tan^2\theta \sin^2\varphi - 2\hat{C}_{23} \tan\theta \sin\varphi\right] . \tag{A-6c}$$

where

$$\hat{C}_{11} = a^2 \cos^2\psi + \sin^2\psi \left(b^2 \sin^2\delta + \cos^2\delta\right) \tag{A-7a}$$

$$\hat{C}_{22} = b^2 \cos^2\delta + \sin^2\delta \tag{A-7b}$$

$$\hat{C}_{33} = a^2 \sin^2\psi + \cos^2\psi \left(b^2 \sin^2\delta + \cos^2\delta\right) \tag{A-7c}$$

$$\hat{C}_{12} = \left(b^2 - 1\right) \sin\psi \sin\delta \cos\delta \tag{A-7d}$$

$$\hat{C}_{13} = \left(a^2 - b^2 \sin^2\delta - \cos^2\delta\right) \sin\psi \cos\psi \tag{A-7e}$$

$$\hat{C}_{23} = -\left(b^2 - 1\right) \cos\psi \sin\delta \cos\delta \; . \tag{A-7f}$$

For the scatter-component calculations we have used the limiting forms of Eqs. (A-5) and (A-6) as $\beta \to 0$. By using the small-argument forms of K_γ (viz, $K_\gamma(2x) \sim \frac{1}{2}\Gamma(\gamma)\, x^{-\gamma}$), we have

$$R_s(y) = 2\left[\frac{y}{2\alpha}\right]^{\gamma-\frac{1}{2}} K_{\gamma-\frac{1}{2}}(y/\alpha)/\Gamma(\gamma-\tfrac{1}{2}) \qquad \text{(A-8)}$$

and

$$\kappa_s = \alpha\, 2\sqrt{\pi}\Gamma(\gamma-\tfrac{1}{2})/\Gamma(\gamma-1) \quad . \qquad \text{(A-9)}$$

Equations (A-1) through (A-7) together with the limiting forms of Eqs. (A-8) and (A-9) constitute a complete characterization of the integrated phase along the principal raypath, which is the starting point for phase-screen calculations.

The spectral density function for phase has the form

$$\Phi_\phi(\vec{K}) = r_e^2 \lambda^2\, \Delta L\, \sec^2\theta\, \Phi_{\Delta N_e}\left(\vec{K},\, -\tan\theta\, \hat{a}_{k_T} \cdot \vec{K}\right) \qquad \text{(A-10)}$$

where

$$\Phi_{\Delta N_e}\left(\vec{K},\, -\tan\theta\, \hat{a}_{k_T} \cdot \vec{K}\right) = ab\langle \Delta N_e^2 \rangle Q\left(\left[AK_x^2 + BK_xK_y + CK_z^2\right]^{\frac{1}{2}}\right) \qquad \text{(A-11)}$$

$$Q(q) = (2\pi\,\alpha\beta)^{3/2}\left(1+\frac{(\alpha q)^2}{2}\right)^{-(\gamma+\frac{1}{2})}\;\frac{K_{\gamma+\frac{1}{2}}\left(2\,\frac{\beta}{\alpha}\sqrt{1+\frac{(\alpha q)^2}{2}}\right)}{K_{\gamma-1}\left(2\,\frac{\beta}{\alpha}\right)} \qquad \text{(A-12)}$$

and $\Phi_{\Delta N_e}(\vec{K}, K_z)$ is the three-dimensional spectral density function of the electron density irregularities. When $\alpha >> \beta$ and $2\pi/\alpha < q < 2\pi/\beta$,

$$Q(q) \approx (2\pi)^{3/2}\,\frac{\Gamma(\gamma+1/2)}{\Gamma(\gamma-1)}\,\alpha^3\,\frac{1}{[1+(\alpha q)^2/2]^{\gamma+1/2}} \cdot \qquad \text{(A-13)}$$

In the model we have taken $\gamma = 1.5$, so that $Q(q) \propto \alpha^{-1}\, q^{-4}$. It follows that $\Phi_{\Delta N_e} \propto \langle \Delta N_e \rangle\, \alpha^{-1}\, q^{-4}$. For the focus component we take

$$\langle \Delta N_e^2 \rangle = \alpha_f/\alpha_s\, \langle \Delta N_e^2 \rangle_s \,, \qquad \text{(A-14)}$$

which makes the composite spectral density function essentially a continuous power law except where $2\pi/\beta_f < q < 2\pi/\alpha_s$.

In the computations, the temporal correlation functions are obtained by replacing $\Delta\vec{\rho}$ and Δz in Eq. (A-2) by the relative drift velocities v_x, v_y, and v_z. We have also used the definition

$$v_{eff} = f(\vec{v}_s) \,. \qquad \text{(A-15)}$$

2. Diffraction Calculations for the Scatter Component

In the Gaussian phase-screen model we can easily calculate the correlation functions $R_s(\Delta\vec{\rho}) = \langle uu'^* \rangle$ and $B_s(\Delta\vec{\rho}) = \langle uu' \rangle$ at the edge of the phase screen. Here u is the scalar wave field. The results are:

$$\begin{Bmatrix} R_s(\vec{\Delta\rho}) \\ B_s(\vec{\Delta\rho}) \end{Bmatrix} = \exp\left\{-\sigma_s^2 \Delta L \left[1 \pm R_s(\vec{\Delta\rho})\right]\right\} - \exp\left\{-\sigma_s^2 \Delta L\right\} \qquad \text{(A-16)}$$

where the upper sign is used for R_s and the lower sign for B_s.

The mutual coherence function R_s is propagation-invariant, whereas for $z > 0$,

$$B_s(\vec{\Delta\rho};z) = \iint B_s(\vec{\Delta\rho}')\, F(\vec{\Delta\rho} - \vec{\Delta\rho}')\, d\vec{\Delta\rho}' \qquad \text{(A-17a)}$$

where

$$F(\vec{\xi}) = \frac{i}{2z} \exp\left\{\frac{i}{4z}\left[(M\vec{\xi})_x^2 \cos\theta + (M\vec{\xi})_y^2\right]\right\} \qquad \text{(A-17b)}$$

$$M = \begin{pmatrix} \cos\varphi & \sin\varphi \\ -\sin\varphi & \cos\varphi \end{pmatrix}. \qquad \text{(A-17c)}$$

By making appropriate substitutions and several variable changes, Eq. (A-16a) can be written in the form

$$\begin{Bmatrix} BR_s \\ BI_s \end{Bmatrix} = \frac{2 \exp\left\{-\sigma_s^2 \Delta L\right\}}{\pi Z_N} \int_0^\infty \omega \begin{Bmatrix} \sin \\ \cos \end{Bmatrix} (\omega^2/Z_N)\, G\,(\omega;\vec{y}_N)\, d\omega \qquad \text{(A-18)}$$

where

$$G(\omega;\vec{y}_N) = \frac{1}{2}\int_0^{2\pi} \left[\exp\left\{-\sigma_s^2 L\, f(\omega,\Phi;\vec{y}_N)\, K_1\left(f(\omega,\Phi;\vec{y}_N)\right)\right\} - 1\right] d\Phi \qquad \text{(A-19)}$$

$$f(\omega,\Phi;\vec{y}_N) = \left[\left(\omega\cos\Phi + y_{N_x}\right)^2 + \frac{C_2}{A_2}\left(\omega\sin\Phi + y_{N_y}\right)^2\right]^{1/2} \quad \text{(A-20)}$$

$$Z_N = \frac{4Z\,A_2}{\alpha_s^2\,[AC - B^2/4]} \quad \text{(A-21)}$$

$$\vec{y}_N = \vec{y}_R\left[\frac{A_2}{\alpha^2\,[AC - B^2/4]}\right]^{1/2} \quad \text{(A-22)}$$

$$A_2 = \frac{1}{2}\,[A_1 + C_1 + D_1] \quad \text{(A-23a)}$$

$$C_2 = \frac{1}{2}\,[A_1 + C_1 - D_1] \quad \text{(A-23b)}$$

$$D_1 = \left[(A_1 - C_1)^2 + B_1^2\right]^{1/2} \quad \text{(A-23c)}$$

$$A_1 = C\cos^2\varphi\,\sec^2\theta - B\sin\varphi\cos\varphi\,\sec\theta + A\sin^2\varphi \quad \text{(A-24a)}$$

$$B_1 = -B\cos 2\varphi\,\sec\theta + (A - C\sec^2\theta)\sin 2\varphi \quad \text{(A-24b)}$$

$$C_1 = C\sin^2\varphi\,\sec^2\theta + B\sin\varphi\cos\varphi\,\sec\theta + A\cos^2\varphi \quad \text{(A-24c)}$$

$$\vec{y}_R = M_R\,\vec{y} \quad \text{(A-25)}$$

$$M_R = \begin{pmatrix} \cos\Phi_R & \sin\Phi_R \\ -\sin\Phi_R & \cos\Phi_R \end{pmatrix} \quad \text{(A-26)}$$

$$\tan 2\Phi_R = \frac{B_1}{A_1 - C_1} \quad . \tag{A-27}$$

In the numerical integration performed in BRBIVL, $G(\omega;\vec{y}_N)$ is first evaluated using an adaptive Simpson method for a logarithmically spaced set of ω values. A set of spline coefficients is then generated for these points. For the ω integration, $G(\omega;\vec{y}_N)$ is interpolated using the spline coefficients.

The integration over the ω variable is performed by integrating over a number of cycles of the sin or cos terms and then summing the resultant series. The integration is terminated when the resultant series converges to within a preassigned value.

3. Propagation Calculations for the Focus Component

For the focus component, the relevant quantities are the log-amplitude and phase of the field. These are calculated by using the ray-optics approximation

$$\frac{\partial \chi_f}{\partial \vec{\ell}} \cong \frac{1}{2k} \nabla_\perp^2 \phi_f \quad , \tag{A-28}$$

from which it follows that

$$\langle \chi_f \phi_f' \rangle = \left(\frac{\lambda_z \sec\theta}{4\pi}\right)\left[a_{11}\frac{\partial^2 R_\phi}{\partial \Delta\rho_x^2} + 2a_{12}\frac{\partial^2 R_\phi}{\partial \Delta\rho_x \partial \Delta\rho_y} + a_{22}\frac{\partial^2 R_\phi}{\partial \Delta\rho_y^2}\right] \tag{A-29}$$

and

$$\langle x_f x_f' \rangle = \left(\frac{\lambda_z \sec\theta}{4\pi}\right)^2 \left[a_{11}^2 \frac{\partial^4 R_{\phi_f}}{\partial \Delta\rho_x^4} + 4a_{11}a_{12} \frac{\partial^4 R_{\phi_f}}{\partial \Delta\rho_x^3 \partial \Delta\rho_y} \right.$$

$$\left. + \left(4a_{12}^2 + 2a_{11}a_{22}\right) \frac{\partial^4 R_{\phi_f}}{\partial \Delta\rho_x^2 \partial \Delta\rho_y^2} + 4a_{12}a_{22} \frac{\partial^4 R_{\phi_f}}{\partial \Delta\rho_x^2 \partial \Delta\rho_y^3} + a_{22}^2 \frac{\partial^4 R_{\phi_f}}{\partial \Delta\rho_y^4} \right] . \quad \text{(A-30)}$$

The evaluation of the derivatives is tedious but straightforward. The results are summarized in Figure A-1, which is a partial listing of the subroutine RFOC. The variable names in the code are self explanatory.

4. Calculation of Intensity and Phase Moments for Composite Signal

The phase autocorrelation function is a simple superposition of Eqs. (A-1) and (A-8). The intensity autocorrelation function R_{I_s} for the scatter component is given in terms of R_s and B_s, from Eq. (A-16), as

$$R_{I_s}(\vec{\Delta\rho}) - 1 = 4R_{xx}(\vec{\Delta\rho})\left(1 - \sigma_{T_s}^2\right) + \left|R_s(\vec{\Delta\rho})\right|^2 + \left|B_s(\vec{\Delta\rho})\right|^2 \quad \text{(A-31)}$$

where

$$\sigma_{T_s}^2 = 1 - \exp\left\{-\sigma_s^2 \Delta L\right\} \quad \text{(A-32)}$$

and

$$R_{xx} = \frac{1}{2}\left[R_s + BR_s\right] . \quad \text{(A-33)}$$

```
C
C       COMPUTE HIGHER ORDER DERIVATIVES OF PHASE AUTOCORRELATION FUNCTION
C       FOR FOCUS COMPONENT
C
        DYKDY=-ARGY*BK0Y
        D2YKDY2=ARGY*BK1Y-BK0Y
        D3YKDY3=-ARGY*BK0Y+BK1Y
        D4YKDY4=ARGY*BK1Y-2.0*BK0Y-BK1Y/ARGY
C
C                       ***************************************************
        TMP1=2.0*BETAF/ALPHAF
        TMP2=2.0*BETAF*BETAF
        TMP3=1.0+F2/TMP2
        TMP4=SQRT(TMP3)
        TMP5=2.0*TMP4*TMP2
        TMP52=TMP5*TMP5
        TMP53=TMP5*TMP52
        TMP54=TMP5*TMP53
C
C                       ***************************************************
        DYDRX=DF2DRX/TMP5*TMP1
        DYDRY=DF2DRY/TMP5*TMP1
        D2YDRXY=(DF2DRX*DF2DRY*(-1.0/(TMP52*TMP4))+D2F2DXY/TMP5)*TMP1
        D2YDRX2=(DF2DRX*DF2DRX*(-1.0/(TMP52*TMP4))+D2F2DX2/TMP5)*TMP1
        D2YDRY2=(DF2DRY*DF2DRY*(-1.0/(TMP52*TMP4))+D2F2DY2/TMP5)*TMP1
        D3YDX2Y=(DF2DRX*DF2DRX*DF2DRY*(3.0/(TMP53*TMP3))+(D2F2DX2
     A      *DF2DRY+2.0*DF2DRX*D2F2DXY)*(-1.0/(TMP52*TMP4)))*TMP1
        D3YDXY2=(DF2DRY*DF2DRY*DF2DRX*(3.0/(TMP53*TMP3))+(D2F2DY2
     A      *DF2DRX+2.0*DF2DRY*D2F2DXY)*(-1.0/(TMP52*TMP4)))*TMP1
        D3YDX3 =(DF2DRX*DF2DRX*DF2DRX*(3.0/(TMP53*TMP3))-3.0*D2F2DX2
     A      *DF2DRX*(-1.0/(TMP52*TMP4)))*TMP1
        D3YDY3 =(DF2DRY*DF2DRY*DF2DRY*(3.0/(TMP53*TMP3))-3.0*D2F2DY2
     A      *DF2DRY*(-1.0/(TMP52*TMP4)))*TMP1
        D4YX2Y2=(DF2DRX**2*DF2DRY**2*(-15.0/(TMP54*TMP3*TMP4))+(4.0*
     A      DF2DRX*D2F2DXY*DF2DRY+DF2DRX**2*D2F2DY2+D2F2DX2*DF2DRY**2)*
     B      (3.0/(TMP53*TMP3))+(D2F2DX2*D2F2DY2+2.0*D2F2DXY**2)*(-1.0/
     C      (TMP52*TMP4)))*TMP1
        D4YDX3Y=(DF2DRX**3*DF2DRY*(-15.0/(TMP54*TMP3*TMP4))+
     A      (3.0*DF2DRX*DF2DRY*D2F2DX2+3.0*DF2DRX**2*D2F2DXY)*(3.0/
     B      (TMP53*TMP3))+3.0*D2F2DX2*D2F2DXY*(-1.0/(TMP52*TMP4)))*TMP1
        D4YDXY3=(DF2DRY**3*DF2DRX*(-15.0/(TMP54*TMP3*TMP4))+
     A      (3.0*DF2DRY*DF2DRX*D2F2DY2+3.0*DF2DRY**2*D2F2DXY)*(3.0/
     B      (TMP53*TMP3))+3.0*D2F2DY2*D2F2DXY*(-1.0/(TMP52*TMP4)))*TMP1
        D4YDRX4=(DF2DRX**4*(-15.0/(TMP54*TMP3*TMP4))+6.0*DF2DRX**2*D2F2DX2
     A      *(3.0/(TMP53*TMP3))+3.0*D2F2DX2**2*(-1.0/(TMP52*TMP4)))*TMP1
        D4YDRY4=(DF2DRY**4*(-15.0/(TMP54*TMP3*TMP4))+6.0*DF2DRY**2*D2F2DY2
     A      *(3.0/(TMP53*TMP3))+3.0*D2F2DY2**2*(-1.0/(TMP52*TMP4)))*TMP1
C
C                       ***************************************************
        CON=BKONE*TMP1
        DRDX=DYKDY*DYDRX/CON
        D2RDY2=(D2YKDY2*DYDRY**2+DYKDY*D2YDRY2)/CON
        D2RDXY=(D2YKDY2*DYDRX*DYDRY+DYKDY*D2YDRXY)/CON
C       D3RDX2Y=(D3YKDY3*DYDRX**2*DYDRY+2.0*D2YKDY2*DYDRX*D2YDRXY
C    A      +D2YKDY2*DYDRY*D2YDRX2+DYKDY*D3YDX2Y)/CON
C       D3RDXY2=(D3YKDY3*DYDRY**2*DYDRX+2.0*D2YKDY2*DYDRY*D2YDRXY
C    A      +D2YKDY2*DYDRX*D2YDRY2+DYKDY*D3YDXY2)/CON
C       D3RDX3=(D3YKDY3*DYDRX**3+3.0*D2YKDY2*DYDRX*D2YDRX2+DYKDY*D3YDX3)/
C    A      CON
C       D3RDY3=(D3YKDY3*DYDRY**3+3.0*D2YKDY2*DYDRY*D2YDRY2+DYKDY*D3YDY3)/
C    A      CON
        D4RDX3Y=(D4YKDY4*DYDRX**3*DYDRY+D3YKDY3*(3.0*D2YDRX2*DYDRX*
     A      DYDRY+3.0*DYDRX**2*D2YDRXY)+D2YKDY2*(3.0*D2YDRX2*D2YDRXY
     B      +3.0*DYDRX*D3YDX2Y+DYDRY*D3YDX3)+DYKDY*D4YDX3Y)/CON
        D4RDXY3=(D4YKDY4*DYDRY**3*DYDRX+D3YKDY3*(3.0*D2YDRY2*DYDRX*
     A      DYDRY+3.0*DYDRY**2*D2YDRXY)+D2YKDY2*(3.0*D2YDRY2*D2YDRXY
     B      +3.0*DYDRY*D3YDXY2+DYDRX*D3YDY3)+DYKDY*D4YDXY3)/CON
        D4RX2Y2=(D4YKDY4*DYDRX**2*DYDRY**2+D3YKDY3*(4.0*DYDRX*DYDRY*
     A      D2YDRXY+DYDRX**2*D2YDRY2+DYDRY**2*D2YDRX2)+D2YKDY2*(2.0 *
     B    D2YDRXY**2+2.0*DYDRX*D3YDXY2+D2YDRY2*D2YDRX2+2.0*DYDRY*D3YDX2Y)
     C      +DYKDY*D4YX2Y2)/CON
        D4RDX4=(D4YKDY4*DYDRX**4+D3YKDY3*6.0*DYDRX**2*D2YDRX2+D2YKDY2*(
     A      3.0*D2YDRX2**2+4.0*DYDRX*D3YDX3 )+DYKDY*D4YDRX4)/CON
        D4RDY4=(D4YKDY4*DYDRY**4+D3YKDY3*6.0*DYDRY**2*D2YDRY2+D2YKDY2*(
     A      3.0*D2YDRY2**2+4.0*DYDRY*D3YDY3 )+DYKDY*D4YDRY4)/CON
C
C                       ***************************************************
```

FIGURE A-1 CALCULATION FOR HIGHER-ORDER PHASE DERIVATIVES

When $\vec{\Delta\rho} = 0$, $R_{I_s}(\hat{o}) - 1$, reduces to the intensity scintillation index S_4^2 for the scatter component.

For the focus component, the corresponding autocorrelation function is

$$R_{I_f}(\vec{\Delta\rho}) = \exp\left\{4\langle\chi_f\chi_f'\rangle\right\} \tag{A-34}$$

where $\langle\chi_f\chi_f'\rangle$ is evaluated by using Eq. (A-30). As with the scatter component, when $\vec{\Delta\rho} = 0$, $S_{4_f}^2 = R_{I_f}(o) - 1$.

The composite intensity autocorrelation function is given as:

$$R_I(\vec{\Delta\rho}) = R_{I_s} R_{I_f} \quad . \tag{A-35}$$

The intensity scintillation index is given as

$$S_4^2 = \left(S_{4_s}^2 + 1\right)\left(S_{4_f}^2 + 1\right) - 1 \quad . \tag{A-36}$$

The phase scintillation index for the focus component is given approximately by $\sigma_f^2\Delta L - \sigma_\chi^2$. This approximation is valid in the presence of weak focusing. For the scatter component, a value consistent with Eq. (A-31) is obtained by integrating the phase distribution function as described in the next subsection.

5. Phase Statistics for the Scatter Component--The Hatfield Distribution

If x and y are jointly Gaussian but otherwise arbitrary random variables, then

$$P_{\phi}(\phi) = \int_{0}^{\infty} a\, P_{xy}(a\cos\phi,\ a\sin\phi)\, da \qquad \text{(A-37)}$$

is the phase probability density function, where $P_{xy}(.,.)$ is the joint probability density for the quadrature components x and y. The form of $P_{xy}(.,.)$ is well known, and it has been shown by Hatfield (Hatfield and Rino, 1975) that $P_{\phi}(\phi)$ admits the closed-form solution

$$P_{\phi}(\phi) = \frac{\exp\left\{-y_x^2/\sigma_x^2 - y_y^2/\sigma_y^2 + f_2^2(\phi)\right\}}{2\pi\,\sigma_x\sigma_y\sqrt{1-\rho^2}\,f_1^2(\phi)}$$

$$\times\left\{(1-\rho^2)\exp\left[\frac{-f_2^2(\phi)}{2(1-\rho^2)}\right] + f_2(\phi)\frac{\sqrt{2\pi-(1-\rho^2)}}{2}\,\mathrm{erfc}\left[\frac{-f_2(\phi)}{\sqrt{2(1-\rho^2)}}\right]\right\} \qquad \text{(A-38)}$$

where

$$f_1(\phi) = \sqrt{\cos^2\phi/\rho_x^2 - 2\rho\cos\phi\sin\phi\,(\sigma_x\sigma_y) + \sin^2\phi/\sigma_y^2} \qquad \text{(A-39)}$$

$$f_2(\phi) = y_x\left\{\cos\phi/\sigma_x^2 - \rho\sin\phi/(\sigma_x\sigma_y)\right\}/f_1(\phi)$$

$$+ y_y\left\{\sin\phi/\sigma_y^2 - \rho\cos\theta/(\sigma_x\sigma_y)\right\}/f_1(\phi) \qquad \text{(A-40)}$$

and σ_x, σ_y, and σ_{xy} are the individual variances of x and y, and σ_{xy} is their covariance. The parameters η_x and η_y are the mean values. Finally,

$$\rho = \sigma_{xy}/\sigma_x\sigma_y \ . \qquad \text{(A-41)}$$

To obtain the rms phase for the scatter component, the Hatfield distribution, Eq. (A-38), is numerically integrated in Subroutine CP RMS. The distribution itself is evaluated in Subroutine PHAS.

6. Two-Frequency Correlation Function

The two-frequency correlation function for intensity is a straightforward extension of Eqs. (A-31), (A-34), and (A-35) in Section 4 of this appendix. For the scatter component we have

$$\langle I_s^{(1)} I_s^{(2)} \rangle - 1 = 4\langle x_s^{(1)} x_s^{(2)} \rangle \eta_x^{(1)} \eta_x^{(2)} + \left| R_s\left(\frac{\Delta f}{f}; z\right) \right|^2 + \left| B_s\left(\frac{\Delta f}{f}; z\right) \right|^2 \tag{A-42}$$

where the superscripts refer to the frequencies $f^{(1)} = f - \Delta f$ and $f^{(2)} = f + \Delta f$. The correlation functions $R_s(\frac{\Delta f}{f}; z)$ and $B_s(\frac{\Delta f}{f}; z)$ are computed from a generalization of Eq. (A-17) in Section 2 of this appendix.

It can be shown that

$$\begin{Bmatrix} R_s\left(\frac{\Delta f}{f}; z\right) \\ B_s\left(\frac{\Delta f}{f}; z\right) \end{Bmatrix} = \iint \begin{Bmatrix} R_s(\Delta\vec{\rho}') \\ B_s(\Delta\vec{\rho}') \end{Bmatrix} F\left(\Delta\vec{\rho} - \Delta\vec{\rho}'; \frac{\Delta f}{f}\right) d\Delta\vec{\rho}' \tag{A-43}$$

where $F(\vec{\xi})$ is computed from Eq. (A-17b) in Section 2 with Z replaced by

$$Z = \begin{cases} \dfrac{\lambda z}{4\pi} \left[\dfrac{\frac{\Delta f}{f}}{1 - \left(\frac{\Delta f}{f}\right)^2} \right] & \text{for } R_s \\ \dfrac{\lambda z}{4\pi} \left[\dfrac{1}{1 - \left(\frac{\Delta f}{f}\right)^2} \right] & \text{for } B_s \end{cases} \tag{A-44}$$

In Eq. (A-44), λ is evaluated at the center frequency $f = (f^{(1)} + f^{(2)})/2$. The input correlation functions R and B are given by Eq. (A-16) with σ_s^2 replaced by

$$\sigma_s^2 = \frac{1}{1 - \left(\frac{\Delta f}{f}\right)^2} \quad . \tag{A-45}$$

Finally,

$$\langle x^{(1)} x^{(2)} \rangle = \tfrac{1}{2} \left[\mathrm{Re}\left\{ R\left(\frac{\Delta f}{f}\right) \right\} + \mathrm{Re}\left\{ B\left(\frac{\Delta f}{f}\right) \right\} \right] \quad . \tag{A-46}$$

For the focus component, Eq. (A-30) in Section 3 is used with λ replaced by $\sqrt{\lambda_1 \lambda_2}$. The correlation coefficient computed is

$$C_{f_1 f_2} \triangleq \left[\frac{\langle I^{(1)} I^{(2)} \rangle}{\langle I^{(1)2} \rangle^{\frac{1}{2}} \langle I^{(2)2} \rangle^{\frac{1}{2}}} \right]^{\frac{1}{2}} \quad , \tag{A-47}$$

which varies between 1 for perfect correlation and $\left[\left(1 + S_4^{(1)2}\right)\left(1 + S_4^{(2)2}\right)\right]^{-1/4}$ if the two frequencies are completely decorrelated. This possibly confusing variation occurs because the average value of intensity is unity, independent of the scintillation level. Thus, $C_{f_1 f_2}$ measures the correlation between intensity fluctuations at the two frequencies rather than the correlation between the total intensities.

7. The Empirical RMS Electron Density Model

The rms electron density, ΔN, is calculated in RMSDN as

$$\Delta N = \Delta N_E + \Delta N_M + \Delta N_H + \Delta N_A \tag{A-48}$$

where the subscripts refer to equatorial, midlatitude, high latitude, and auroral respectively. Each term is given as a function of mean sunspot number, R, geomagnetic latitude, λ_m, day of year, D ($1 \leq D \leq 365$), time of day in decimal hours, and the planetary magnetic index, K_p, as follows:

$$\Delta N_E = 2.3 \times 10^9 (1 + 0.04\ R) \left\{ \exp - \left[\frac{(\lambda_m - 10^\circ)^2}{(10^\circ)^2} \right] + \exp \left[- \frac{(\lambda_m + 10^\circ)^2}{(10^\circ)^2} \right] \right\}$$

$$\left\{ 1 - 0.4 \left[\cos \frac{\pi(D + 10)}{91} + \frac{\lambda_g}{15^\circ} \cos \frac{\pi(D + 10)}{182} \right] \right\}$$

$$\left\{ \exp \left[- \frac{(T + 1.5)^2}{(6)^2} \right] + \exp \left[- \frac{(T - 22.5)^2}{T_R^2} \right] \right\} \text{el/m}^3 \qquad \text{(A-49a)}$$

where

$$T_R = \begin{Bmatrix} 3 \\ 6 \end{Bmatrix} \text{ if } T \gtrless 22.5 \qquad \text{(A-49b)}$$

$$\Delta N_M = 1.3 \times 10^9 \left(1 + 0.33 \cos \frac{\pi T}{12} \right) \exp \left[- \frac{(\lambda_m - 32.5)^2}{(15^\circ)^2} \right] \text{el/m}^3 \qquad \text{(A-50)}$$

$$\Delta N_H = 3 \times 10^9 \left(1 + \text{erf} \frac{\lambda_m - \lambda_b}{\lambda_h} \right) \text{el/m}^3 \qquad \text{(A-51a)}$$

$$\lambda_b = 68.5 - 1.8\ K_p - (5 + 0.5\ K_p) \cos \frac{\pi T}{12} \text{ deg} \qquad \text{(A-51b)}$$

$$\lambda_h = 5 + 0.2\,\lambda_b \text{ deg} \tag{A-51c}$$

$$\Delta N_A = 3.2 \times 10^8\, K_p \exp\left[-\frac{(\lambda_m - \lambda_a)^2}{(1.1\,K_p)^2}\right] \text{el/m}^3 \tag{A-51d}$$

$$\lambda_a = 74 - 1.8\,K_p - 4\cos\frac{\pi T}{12} \text{ deg} \tag{A-51e}$$

with

- R = Mean sunspot number
- λ_m = Geomagnetic latitude
- λ_g = Geographic latitude
- D = Day out of 365
- T = Time of day in decimal hours
- K_p = Planetary magnetic index.

All parameters in the model refer to F-layer penetration point.

In the subroutines, MDLPRM, additional parameters that vary with latitude are computed. They are the elongation parameters a and b, the outer scale for the focus component, α_f, the layer thickness, L, and the layer height, H. The specific formulas are

$$a = 30 - 10\left(1 - \text{erf}\left[\frac{\lambda_m - 20^\circ}{3^\circ}\right]\right) \tag{A-52}$$

$$b = 1 + 2.5\left(1 + \text{erf}\left[\frac{\lambda_m - \lambda_b}{3^\circ}\right]\right) \tag{A-53}$$

$$\alpha_f = 900 + 850\left(1 + \text{erf}\left[\frac{\lambda_m - 20^\circ}{3^\circ}\right]\right) \text{m} \tag{A-54}$$

$$L = 200 - 50\left(1 + \text{erf}\left[\frac{\lambda_m - 20^\circ}{3^\circ}\right]\right) \text{ km} \qquad \text{(A-55)}$$

$$H = 500 - 75\left(1 + \text{erf}\left[\frac{\lambda_m - 20^\circ}{3^\circ}\right]\right) \text{ km} . \qquad \text{(A-56)}$$

The remaining scale parameters, β_f and α_s, are given in terms of α_f as

$$\beta_f = \alpha_f/2.5 \qquad \text{(A-57a)}$$

$$\alpha_s = \alpha_f/4 . \qquad \text{(A-57b)}$$

8. Coordinate Transformations

All diffraction calculations are performed in a downward-directed local geomagnetic coordinate system. The receiver coordinate system is upward-directed and tangent to the earth's surface. For characterizing the spatial structure of the field, it is necessary to convert from one coordinate system to the other. The two coordinate systems are shown in Figure A-2.

The coordinate rotation that takes the receiver systems parallel to xyz is

$$\vec{x} = R\,\vec{x}_p \qquad \text{(A-58)}$$

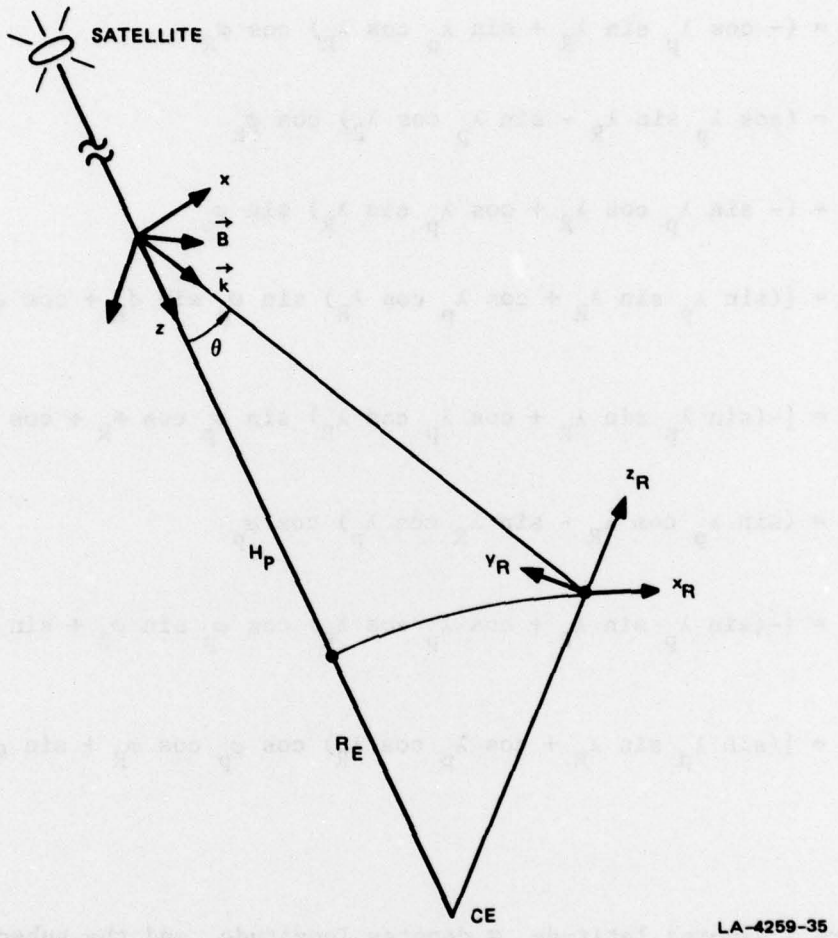

FIGURE A-2 RELATION BETWEEN LOCAL GEOMAGNETIC COORDINATE SYSTEM AND RECEIVER COORDINATE SYSTEM. x-z is the plane of the local magnetic meridian; y_R points true north.

where $\vec{x} = (x, y, z)^T$, $\vec{x}_p = (x_p, y_p, z_p)^T$, and the matrix R has elements

$$R_{11} = \cos \lambda_p \cos \lambda_R + \sin \lambda_p \sin \lambda_R \quad \text{(A-59a)}$$

$$R_{12} = (- \cos \lambda_p \sin \lambda_R + \sin \lambda_p \cos \lambda_R) \cos \varphi_R \quad \text{(A-59b)}$$

$$R_{13} = (\cos \lambda_p \sin \lambda_R - \sin \lambda_p \cos \lambda_R) \cos \varphi_R \quad \text{(A-59c)}$$

$$R_{21} = (- \sin \lambda_p \cos \lambda_R + \cos \lambda_p \sin \lambda_R) \sin \varphi_p \quad \text{(A-59d)}$$

$$R_{22} = [(\sin \lambda_p \sin \lambda_R + \cos \lambda_p \cos \lambda_R) \sin \varphi_p \sin d_R + \cos \varphi_p \cos \varphi_R] \quad \text{(A-59e)}$$

$$R_{23} = [-(\sin \lambda_p \sin \lambda_R + \cos \lambda_p \cos \lambda_R) \sin \varphi_p \cos \varphi_R + \cos \varphi_p \sin \varphi_R] \quad \text{(A-59f)}$$

$$R_{31} = (\sin \lambda_p \cos \lambda_R - \sin \lambda_R \cos \lambda_p) \cos \varphi_p \quad \text{(A-59g)}$$

$$R_{32} = [-(\sin \lambda_p \sin \lambda_R + \cos \lambda_p \cos \lambda_R) \cos \varphi_p \sin \varphi_R + \sin \varphi_p \cos \varphi_R] \quad \text{(A-59h)}$$

$$R_{33} = [(\sin \lambda_p \sin \lambda_R + \cos \lambda_p \cos \lambda_R) \cos \varphi_p \cos \varphi_R + \sin \varphi_p \sin \varphi_R] \quad \text{(A-59i)}$$

where λ denotes latitude, φ denotes longitude, and the subscripts p and R denote penetration point and receiver, respectively.

The rotation to local geomagnetic coordinates is

$$x = \sin \delta x_p + \cos \delta y_p \quad \text{(A-60a)}$$

$$y = \cos \delta x_p - \sin \delta y_p \quad \text{(A-60b)}$$

where δ is the magnetic declination angle. We note that $R^{-1} = R^T$. The superscript T denotes transpose. To characterize the spatial autocorrelation function at the receiver, we use the transformation

$$\Delta x = (M_{11} \sin \delta + M_2, \cos \delta)\, \Delta x_R + (M_{12} \sin \delta - M_{21} \sin \delta)\, \Delta x_R \tag{A-61a}$$

$$\Delta y = (M_{11} \cos \delta - M_{21} \sin \delta)\, \Delta x_R + (M_{12} \cos \delta - M_{22} \sin \delta)\, \Delta y_R \tag{A-61b}$$

$$\Delta z = - M_{31}\, \Delta x_R - M_{32}\, \Delta y_R \ . \tag{A-61c}$$

The family of ellipses generated by $f(\Delta\vec{\rho}_s) = \text{const.}$ is characterized by the orientation angle

$$\phi_E = 1/2 \arctan \left[\frac{B}{A - C}\right] \tag{A-62}$$

measured counterclockwise from the x-axis to the semi-major axis of the ellipse. The axial ratio is

$$AR = [(A + C + D)/(A + C - D)]^{\frac{1}{2}} \tag{A-63}$$

where

$$D = [(A - C)^2 + B^2]^{\frac{1}{2}} \ . \tag{A-64}$$

Since we are using a downward-directed geomagnetic coordinate system, the x-axis points in the magnetic southward direction. To calculate the anisotropy in the receiver plane, the coefficients C, -B, and A in Eqs. (A-62), (A-63), (A-64) are replaced by the coefficients of Δx_R^2, $\Delta x_R \Delta y_R$, and Δy_R^2, respectively.

9. The Nominal Orbit Code

A satellite in circular orbit is easily described mathematically. The relevant parameters are shown in Figure A-3. Within the orbit plane

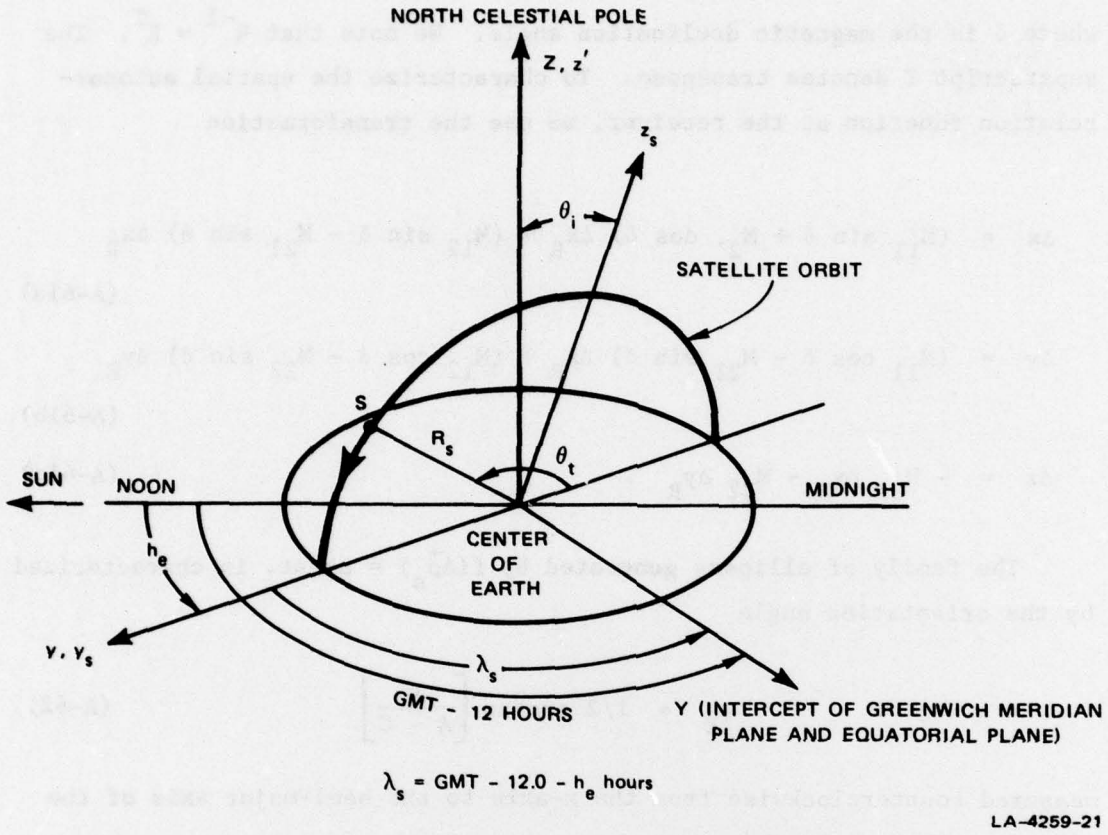

FIGURE A-3 GEOMETRY OF SATELLITE ORBIT

the satellite position is determined by the time, t, the orbital period, τ, and a time parameter, t_o, which determines the time of the equator plane crossing. The orbit plane itself is located by two angles--namely, the inclination relative to the north celestial pole, θ_i, and the location of the orbit plane relative to the sun, h_e, which we take to be fixed.

The position of the satellite in the earth-centered system XYZ shown in Figure A-3 is

$$X = R_s(-\cos \lambda_s(t) \sin \theta_i \sin \theta(t) - \sin \lambda_s(t) \cos \theta(t)) \quad \text{(A-65a)}$$

$$Y = R_s(\sin \lambda_s(t) \sin \theta_i \sin \theta(t) - \cos \lambda_s(t) \cos \theta(t)) \quad \text{(A-65b)}$$

$$Z = R_s \cos \theta_i \sin \theta(t) \quad \text{(A-65c)}$$

where

$$\lambda_s(t) = \frac{2\pi}{24}(t - 12 - h_e) \tag{A-66}$$

and

$$\theta(t) = \frac{2\pi 60}{\tau}(t - t_o) \quad . \tag{A-67}$$

The orbital period and R_s are related by the orbit equation

$$\tau = 2\pi \left[\frac{R_s^3}{m_e G}\right]^{\frac{1}{2}} \Big/ \; 60 \quad . \tag{A-68}$$

In Eq. (A-68), m_e is the mass of the earth and G is the gravitation constant.

From Eqs. (A-65a) through (A-66), one can show that the latitude and longitude of the satellite are given by the formulas

$$\text{SLAT}(t) = \arctan\left\{\sin\theta(t)\cos\theta_i,\ [\cos^2\theta(t) + \sin^2\theta_i \sin\theta(t)]\right\} \tag{A-69}$$

$$\text{SLON}(t) = \arctan\Big\{-\left(\sin\theta_i \sin\theta(t)\cos\lambda(t) + \cos\theta(t)\sin\lambda(t)\right),$$
$$\left(\cos\theta(t)\cos\lambda(t) - \sin\theta_i \sin\theta_i(t)\sin\lambda(t)\right)\Big\}. \tag{A-70}$$

respectively. In subroutine FINDORB, Eqs. (A-69) and (A-70) are solved iteratively for the orbital parameters τ, h_e, and θ_i, for a given period τ and a set of two points on the earth. A reference time is specified for the first point.

The algorithm allows the user to generate a local circular orbit that will approximate the trajectory of any actual satellite, at least over a small interval.

Once the orbit is specified, it is straightforward to calculate the satellite scan velocity $\vec{v}_s$, which is usually the dominant contribution to the time structure of the signal. The routine is useful in general for generating parameter variations that are representative of the various typical orbiting satellite conditions a user might encounter.

REFERENCES

Fremouw, E.J. and C.L. Rino, "Modeling of Transionospheric Radio Propagation," Final Quarterly Technical Report, Contract F30602-74-C-0279, SRI Project 3416, Stanford Research Institute, Menlo Park, California (1975), A023197.

Fremouw, E.J. and C.L. Rino, "Continued Modeling of Transionospheric Radio Propagation," Quarterly Technical Report 3, Contract F30602-75-C-0236, SRI Project 4259, Stanford Research Institute, Menlo Park, California (March 1976).

Fremouw, E.J., C.L. Rino, A.R. Hessing, and V.E. Hatfield, "A Transionospheric Communication Channel Model," Quarterly Technical Report 7, Contract F30602-75-C-0236, SRI Project 4259, Stanford Research Institute, Menlo Park, California (July 1977).

Rino, C.L. and E.J. Fremouw, "The Angle Dependence of Singly Scattered Wavefields," submitted to J. Atmos. Terr. Phys. (1977)

Hatfield, V.E. and C.L. Rino, "Non-Rician Statistics and Their Implications for Modeling Effects of Scintillation on Communication Channels," in proceedings, The Effect of the Ionosphere on Space Systems and Communications, J.M. Goodman, ed., Arlington, Virginia, Naval Research Laboratory, Washington, D.C. (20-22 January 1975).